Fracture behavior in a modified Transverse Crack Tension test under compressive stress

A qualitative study on model parameters

in partial fulfillment of the requirements for the degree of

Master of Science

in Civil Engineering
Structural Mechanics

at the Delft University of Technology
to be defended publicly on Thursday March 29, 2018 at 11:00

by

ing. D. de Groot

Thesis committee:	Prof. dr. ir. L.J. Sluys,	TU Delft, Chair
	Dr. ir. F.P. van der Meer,	TU Delft, Supervisor
	Dr. D. Zarouchas,	TU Delft

Acknowledgements

This thesis is the concluding product for me to obtain my Master of Science degree in Civil Engineering at the faculty of Civil Engineering and Geosciences of the Delft University of Technology.

I would like to express my appreciation and gratitude for Dr.ir. F.P. van der Meer and Prof.dr.ir. L.J. Sluys for the opportunity to perform this research at their department and their invaluable support.

I would also like to thank the teaching professors of the Civil Engineering faculty for their inspiration and sharing of their the knowledge, which has allowed me to accomplish this achievement.

And finally, I would like to thank my family, friends and girlfriend for their unquestionable support during my studies in Delft.

ing. Dennis de Groot

Heemskerk, March 2018

Abstract

An increase in apparent mode II fracture toughness in Fiber Reinforced Polymers has been found from modified Transverse Crack Tension (mTCT) tests with compressive stresses added orthogonal to the delamination plane. Numerical reproduction of these results has not yet led to a good understanding of the reasons for this behavior.

Currently, an analytical approach is used for determining the mode II fracture toughness from an mTCT test. In this research, the validity of the analytical relation is investigated for the case of an added compressive stress. The behavior of the material in the test is therefore numerically investigated in a qualitative manner.

A mesh, using a material model for plasticity and a cohesive law for interface elements to form the crack, which have been proven to give good results, has been build. A refinement on mesh and geometrical dimensions, focused on the pressure zone of the specimen, ensures the degree of detail required to investigate the local behavior. A parameter study on the influence of geometrical and material parameters is performed and linked to results from previous conducted experiments.

A standard mTCT test without compressive stress shows a linear load displacement relation until crack initiation and then a constant load at which the crack grows through the specimen. This crack growth load is used for the analytical approach. The results from this research show a change from a constant crack growth load to a linear crack growth load range in the zone of the applied compressive stress. After crack initiation, the crack growth load through the compressed zone has an increasing, nearly linear relation, based on the compressive stress and length of the pressure zone. The analytical approach, in which the highest reached load on the specimen before failure is used as input, no longer applies for this case. The failure load is now dependent on the length of the pressure zone and pressure magnitude.

Contents

Acronyms

ASTM American Society for Testing and Materials. 5

DCB Double Cantilever Beam. 1

ELS End Loaded Split. 1, 5

ENF End Notched Flexure. 1, 5

MMB Mixed Mode Bending. 1

mTCT Modified Transverse Crack Tension. 1, 2, 3, 4, 6, 7, 9, 11, 17, 18, 33

TCT Transverse Crack Tension. 1, 2, 4, 6, 7, 12, 20, 32, 33

List of Figures

List of Tables

Chapter 1

Introduction

1.1 Background

Composite laminates provide the ability of combining materials to reach optimal engineering properties. With this complex positive feature, however, comes an equally complex challenge in defining its possible failure mechanisms. One of these mechanisms is the mode II delamination, in which shear failure occurs between layers. In a structure, these interlaminar cracks arise often due to discontinuities like holes or cutouts. A realistic scenario in which this kind of characteristic failure occurs is near bolted joints.

Multiple material parameters are of interest in delamination analysis, among which the fracture toughness. This is a key parameter in crack propagation in these analysis. Most popular and standardized tests to determine this parameter are the Double Cantilever Beam (DCB), End Notched Flexure (ENF), End Loaded Split (ELS) and Mixed Mode Bending (MMB) test methods, which assume that the fracture toughness, for a given mode of fracture, is a material property. This assumption is contradicted for the mode II fracture toughness by measurements from the Transverse Crack Tension (TCT) test, as results from previous research Wisnom [1] and van der Meer and Sluys [2] indicate that the fracture toughness as calculated from the TCT test depends on the geometry of the specimen. This size dependence of the results contradicts the assumption of the fracture toughness as a material parameter.

The TCT test has a tendency to give a higher mode II fracture toughness than the ENF test and, as investigated by Scalici et al. [3], fail in an asymmetrical manner, which invalidates the test. Even though the TCT test has these known uncertainties, it remains a relatively simple test compared to the popular test methods. Another favorable quality is the purely tensile failure mode of the specimen, in contrast to the bending loading modes of the standardized tests. To ensure a symmetrical failure mode of the specimen, a modified TCT test was proposed and tested by Scalici et al. [3]. A release film has been added to the specimen to act as a pre-crack, which ensures a symmetrical failure mode.

Added compressive stresses on the laminates from bolts and washers are found to increase the local fracture toughness [4]. This has been investigated using the Modified Transverse Crack Tension (mTCT) test by Catalanotti et al. [5], where a relation between the maximum load and the compressive stress was found for the analytical computation of the mode II fracture toughness.

While good results are achieved when numerically reproducing the experiments, a clear understanding of the local phenomena in the compressed zone is still missing. Besides the impact of the size of the specimen on the results of a TCT test, more variables could be affecting these results when a compressive stress is added to the test. This thesis is aimed at clarifying this.

To get a better understanding of the local mechanisms in and around the compressed

area, a finite element model has been built. The mesh was tested for the influence of its size and the size of its elements on the output, to assure that minimizing the calculation times would not affect the accuracy of the results. The material models that have proven to give accurate results for TCT models as in van der Meer and Sluys [2] have been applied. Using this model, a parameter study was then performed on material as well as geometrical properties to investigate their influence on the apparent fracture toughness of an mTCT test with through the thickness compressive stress. A validation of the model is done by comparing its output to that of the experiments.

1.2 Problem statement

The problem statement of this research is the following:

An apparent increase in fracture toughness in the mTCT test is observed when applying a through the thickness compressive stress at the crack initiation area of a tested specimen, however, it has not been proven that the analytical formula for computing the fracture toughness from TCT test measurements is still valid for the case of added compressive stress.

1.3 Main research question

- Is the analytical approach for the mode II fracture toughness valid for the mTCT test with through the thickness compressive stress?

1.4 Approach

In order to answer the main research question, a more detailed look at the failure mode in the compressed zone is required. To evaluate whether the assumptions of the analytical approach of the fracture toughness match the mechanisms of the failure mode in the compressed zone of the mTCT test, a computational study has been used to find the answers to the following questions.

- What influence do the models material and geometrical parameters have on the output of the model?
- How does a through the thickness compressive stress, applied to a modified Transverse Crack Tension test, influence the results and the apparent fracture toughness of the material?
- How suitable is the numerical model for further research on the through the thickness compressive stress modified Transverse Crack Tension test?

1.5 Outline

This thesis is structured as follows.

In Chapter 2, a description of the fracture toughness of materials and the experiments to determine them is given, followed by an introduction to the TCT and mTCT test, the specifications of the experiment and its results, and the analytical approach of the fracture toughness for this type of test.

In chapter 3, the model and its mesh properties are described, followed by the cohesive law for the interface elements in the cohesive zone, the material model of the bulk material, the results of the parameter study on the length of the model and the mesh refinement study.

In chapter 4, the basis model of the mTCT test without compressive stress is shown as reference, followed by the parameter study on the fracture toughness, the shear strength, the pressure zone length, the compressive stress and the friction, then these results are linked to the experiment data and the important model characteristics are summarized.

In chapter 5, a discussion of the results and the conclusions that can be taken from it are discussed, followed by recommendations for further research.

Chapter 2

Theory, tests and the experiment

In this chapter, some theory and information about the test methods will be given. The concept of the fracture toughness and its failure modes are introduced, along with a description of the standardized tests to measure the mode II fracture toughness. In a more detailed description, the TCT and mTCT test and the analytical approach for them are described, concluding with the experiment setup and results of the mTCT test with compressive stress and the adapted analytical approach.

2.1 Fracture toughness

When considering laminated composites, interlaminar fracture is one of the prominent failure mechanisms. Fracture toughness is the materials capability of resisting the propagation of a crack, which makes it an important input parameter for the calculation of delamination.

2.1.1 Crack separation

Considering the input parameter for the fracture toughness, a basic bilinear relation as shown in Figure 2.1 is used for the application of shear failure in fracture mechanics. A linear relation between the shear stress and strain is applied until the onset criterion at the maximum shear stress. Softening in the material occurs from this point, until the propagation criterion, at which the material has no strength left and a full crack has formed. When the fracture toughness G_c as input parameter is increased, it would result in a less steep softening branch of the diagram and therefore a larger displacement for the propagation criterion.

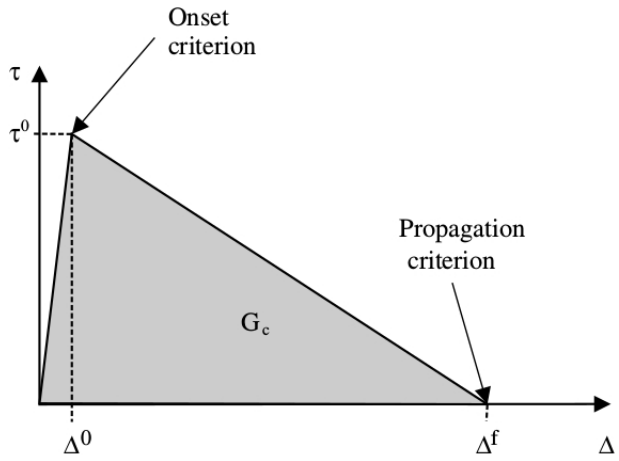

Figure 2.1: Bilinear constitutive relation for decohesion element

The three possible failure modes are identified as mode I, II and III, which are illustrated in Figure 2.2. Mode I has a crack formation due to a tensile stress normal to the plane of the crack. Mode II forms a crack plane parallel to an acting shear stress in a sliding manner. Mode III has a tearing manner of failure, with a shear stress acting parallel to the crack plane. These modes have their own fracture toughness. In practice delamination will often grow in an intermediate mode. A kind of interpolation of fracture toughness as a function of mixed modes is then required.

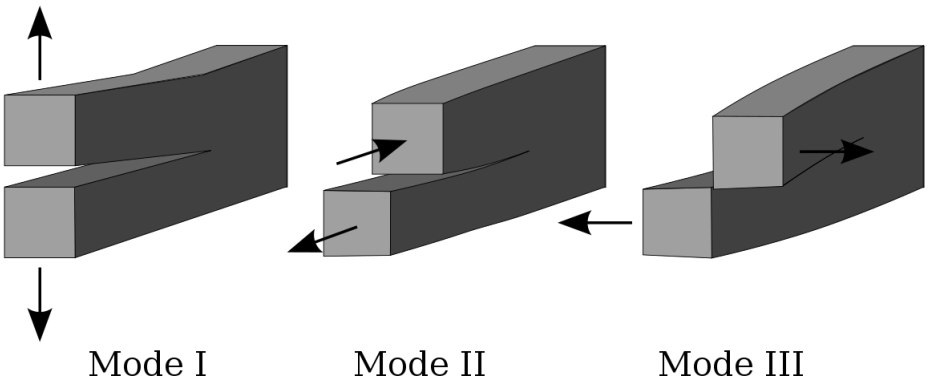

Figure 2.2: The three possible fracture modes

Since most materials have a different fracture toughness per mode, they have to be tested by separate experimental setups, assuring a single mode failure per test.

2.1.2 Standardized tests

Testing of the mode II fracture toughness for laminated composites has been done by different experimental setups through the years. Two tests that have been adopted by the American Society for Testing and Materials (ASTM), are the ENF and ELS test, which are illustrated in Figure 2.3. Both tests are characterized by a point load resulting in bending of the specimen, which in turn results into shear stresses around the crack tip.

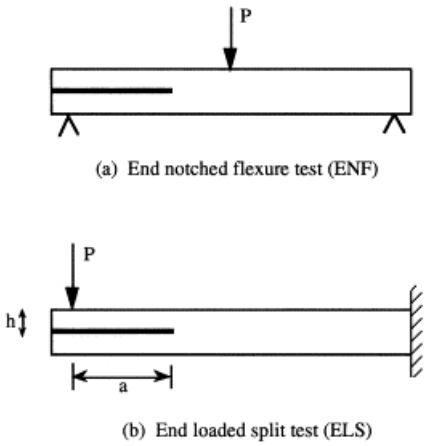

Figure 2.3: Shear driven ENF and ELS test [6]

2.1.3 The TCT test

Comparing the TCT test to the aforementioned standardized tests shows a key difference in how the load is applied. Instead of a shear stress acting on a notch that arises from bending, the shear stresses in a TCT test are induced by global tension. Figure 2.4(a) shows the initial setup of a TCT test, consisting of a specimen with continuous layers on the top and bottom, and discontinuous layers in the center. Increasing the tensional forces on both ends of the specimen induces shear stresses at the tips of the cut in the discontinuous layers, resulting in the formation and propagation of interlaminar cracks 2.4(b).

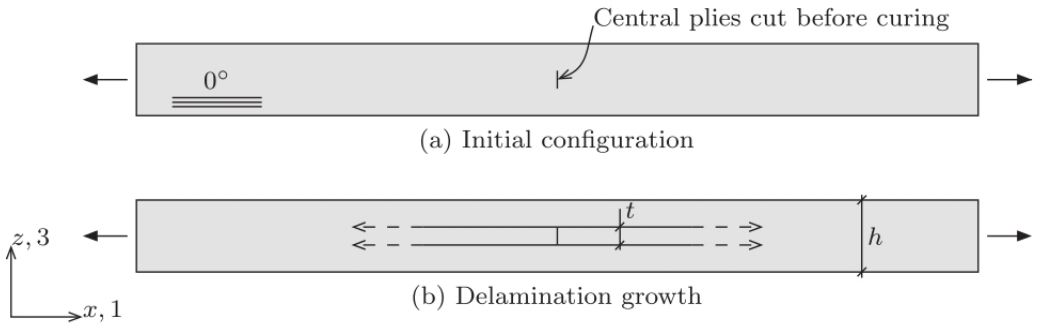

Figure 2.4: TCT test before and after crack formation [2]

Analytical approach

To determine the mode II fracture toughness from the results of a TCT test, the applied formula is Eq. 2.1, with G_{II} the mode II fracture toughness, σ the tensile stress in the specimen at the moment of failure (load drop), found by dividing the tensile force on the specimen by its cross section. E_1 is the youngs modulus in the longitudinal direction, $2H$ the thickness of the specimen and ξ the ratio $2h/2H$ with $2h$ the thickness of the cut plies. The assumption for 2.1 is a constant load during crack propagation. It is therefore applied to the failure load of a TCT test, in which a constant load until failure characterizes the crack growth load.

$$G_{II} = \sigma^2 \frac{H}{2E_1}\left(\frac{1}{\xi} - 1\right) \tag{2.1}$$

2.1.4 The mTCT test

In the experimental campaign conducted by Scalici et al. [3], the results obtained with this configuration could not be used due to asymmetrical failure modes. A solution for this phenomenon was proposed by Scalici et al. [3] in the form of the modified Transverse Crack Tension (mTCT) test, in which there are pre-cracks from the tips of the central cut by use of release films, as can be seen in Figure 2.5. Positive results were achieved from the modified test, in which the failure modes of the specimen were symmetrical, paving the way for the experimental setup for the mTCT test with through the thickness compressive stress.

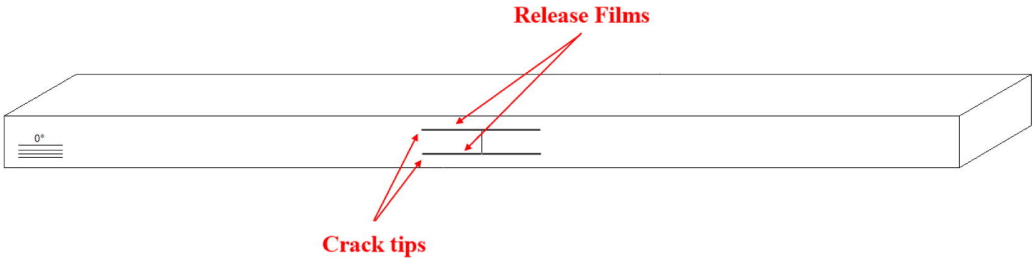

Figure 2.5: mTCT test with release films, acting as pre-cracks [3]

Delamination of a laminated composite which closely resembles the failure mode of a TCT test arises for instance around holes and cutouts. These are often used for connections between elements by bolts and rivets, which in turn apply a compressive stress on the area surrounding the hole due to clamping. It has been shown that these compressive stresses increase the failure load of the material Collings [4]. The exact cause of the increase in fracture toughness is not yet understood, but has been found to be influenced by the compressive load to the material, and its magnitude. To measure this influence, the mTCT test has been augmented by Catalanotti et al. [5] with a compressive stress σ_{33} through the thickness of the specimen, applied to the area around the crack tips as shown in Figure 2.6.

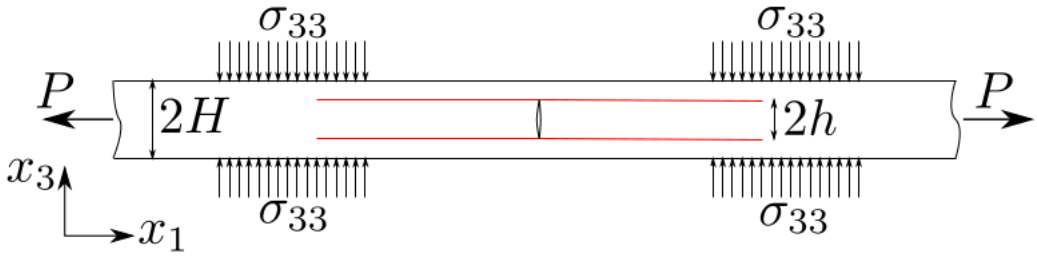

Figure 2.6: Experiment specimen setup

2.2 Experiment setup

In the experimental study by Catalanotti et al. [5], sixteen specimens of cured Hexcel IM7-8552 unidirectional lamina of 300x300 mm^2 were prepared, with a thickness of 4 mm. A layup of $[0_8/*0_{16}/0_8]$ was used, with the '*' denoting the cut plies. Release films were placed between the continuous plies and the cut plies, as characteristic for the mTCT test, functioning as pre-cracks. The specimens were cut to 200x15 mm^2 and placed in the lateral grips as described in [5] and shown in Figure 2.7 to apply the compressive stress. For σ_{33}, five values in a range of 17 to 102 MPa were applied to the specimen, covering

the range that can be expected to occur in the aeronautical industry for bolted joints or tightened filled holes. As can be seen from Figure 2.6, the compressive stress is applied to the area around the crack tips of the pre-cracks, using lateral steel grips with M10 bolts as can be seen in Figure 2.7. The grips were designed to apply a constant uniform stress and prevent out of plane curvature of the specimen throughout the experiment, and used to vary the compressive stresses, controlled by the tightening of the bolts. Applied specimen dimensions, for which no selection process was specified, are as in Table 2.1. Loading of the sample was done by an Instron 4208 testing machine under a displacement controlled 1 mm/min crosshead speed.

Area	[mm]
Sample thickness ($2H$)	4
Continuous plies thickness	2
Cut plies thickness ($2h$)	2
Sample length	200
Sample width	15
Pressure zone length	20
Symmetry axis to pressure zone	25
Length after pressure zone	55

Table 2.1: Specimen dimensions

The compressive stresses of -17, -34, -51, -85 and -102 MPa and the matching test results as found by Catalanotti et al. [5] and in section 2.3, will later in this report be used to compare to the model results. The characteristic response for a fracture toughness test is a load displacement curve with a linear relation until crack initiation. When the beginning of a crack has fully formed, propagation starts. In an ideal situation, crack propagation is denoted by a horizontal load displacement relation until failure. Failure is expected to happen after the crack reaches the end of the compressed zone and results in the experiment as well as the actual situation in a load drop in the load displacement diagram.

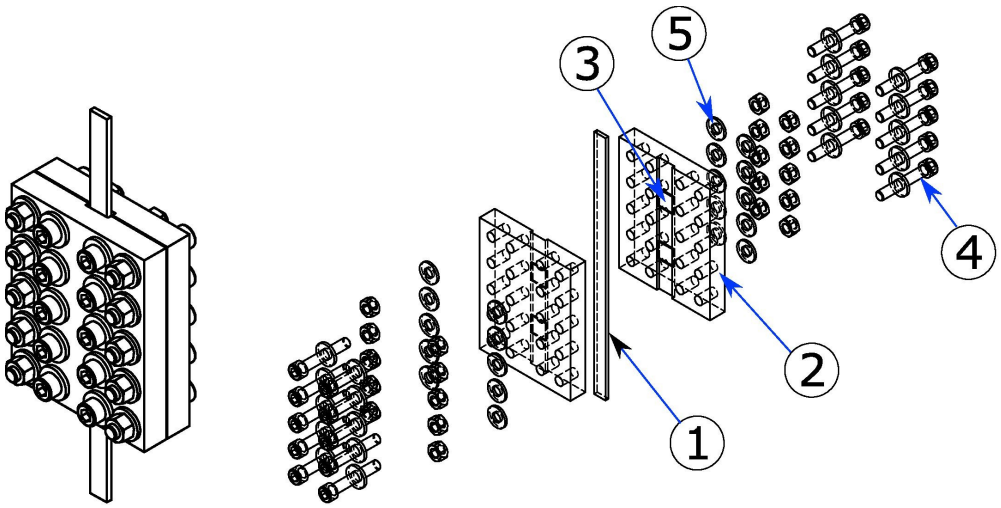

(a) Assembly.

(b) Exploded view: ① specimen, ② lateral grips, ③ teflon inserts, ④ M10 bolts, ⑤ disk washers

Figure 2.7: Steel lateral grips as applied by Catalanotti et al. [5]

2.3 Experiment results

Results from the performed experiments are plotted as load displacement diagrams and shown in Figure 2.8. Of the 16 performed experiments, one load displacement diagram for each of the compressive stresses has been plotted below.

A linear loading branch until sudden failure in the form of a load drop is visible in the results, as characteristic for the mTCT test. There is also an increase in maximum load for the higher compressive stresses, as is previously discussed in [5].

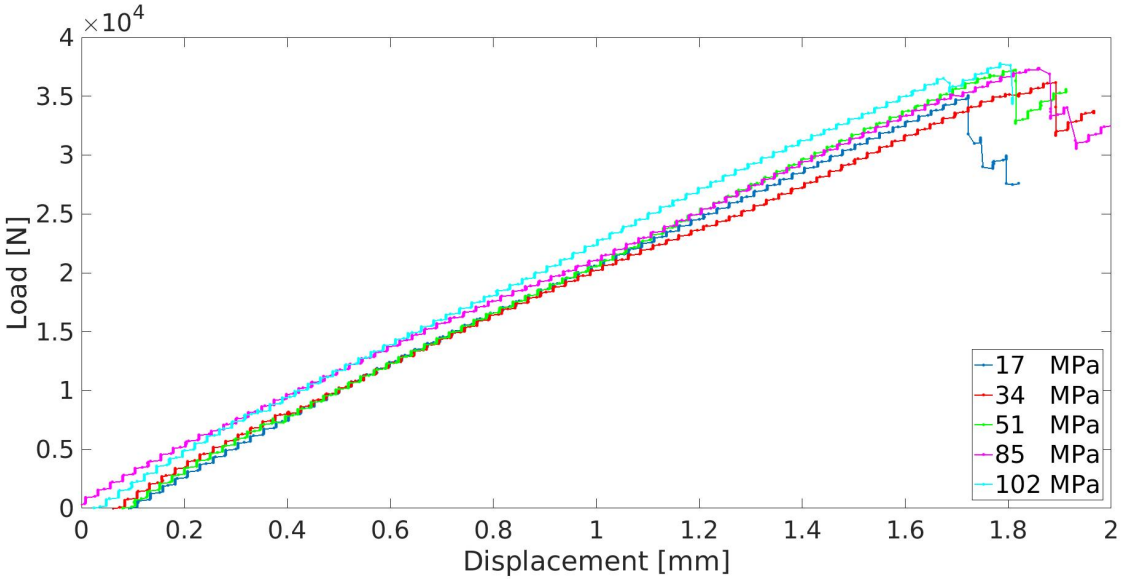

Figure 2.8: Load displacement diagrams of tested specimens

Also reported in the results is the small displacement jump in the diagrams, which arise around the maximum load of the specimen with 17 MPa compressive stress. A closer look at these displacement jumps is shown in Figure 2.9, in which the results from the specimens with the most distinct jumps are plotted.

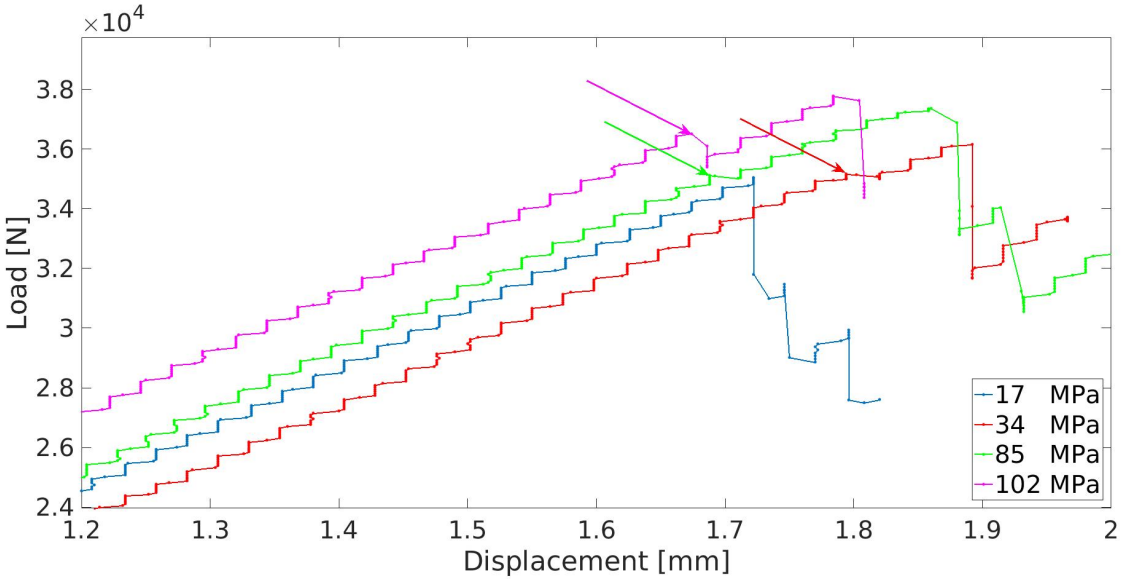

Figure 2.9: Load displacement diagrams with displacement jumps

2.3.1 Adapted analytical approach

After studying the data of the experiments, Catalanotti et al. [5] found a correlation between the failure load and the through the thickness stress. After substituting the tensile stress in the specimen at the moment of failure (load drop), into Eq. 2.1 to find the fracture toughness, Eq. 2.2 shows the derived relation. G^c_{II0} denotes the fracture toughness of the specimen without the through the thickness stress, and η an empirical parameter, fitted to the results.

$$G^c_{II} = G^c_{II0}(1 + \eta\langle -\sigma_{33}\rangle) \tag{2.2}$$

Chapter 3

Model definition

Building the model to reproduce the experimentally investigated influence of compressive stresses as described by Catalanotti et al. [5], which this numerical study has been focused on, is described in this section. Computational efficiency requires the model to be as simple as possible concerning the dimensions of the model and its mesh size, whilst retaining result accuracy. Focus here is on the compressed zone to give a detailed output of the behavior of the model in this area.

This chapter describes the mesh to reproduce the behavior of the test as described in section 2.2. This is followed by the cohesive law as applied to the interface elements for the formation of the crack, and the damage/plasticity model of the bulk material. Then the steps taken to reach a reliable model size are discussed, as symmetry can be applied and not the entire specimen length needs to be modeled. The section is then closed with a mesh refinement study to reduce calculation time to a minimum.

3.1 Model

A mesh has been built in Gmsh for this study, which has then been used in Jem Jive to perform the various calculations on. As the mTCT test lends itself for the use of symmetry over two axes, calculation times can be significantly reduced. To this end, the upper right quarter of the sample has been modeled as shown in Figure 3.1, where the upper half of the mesh shows the continuous plies in the specimen, and the bottom half the discontinuous plies. The specimen is modeled as a continuum with a damage/plasticity model as described in section 3.1.1 for the shear deformations, with linear properties in the normal directions. This can be done for simplicity of the model, as damage in the normal direction will not occur within the amount of displacement of this test. The cut is simulated by the lower half of the left boundary of the model, being able to move freely in the x direction. Prescribing a zero displacement for the continuous plies in the x direction on this boundary of the mesh, and a zero displacement of the bottom boundary of the mesh in the y direction simulates the symmetry of the specimen.

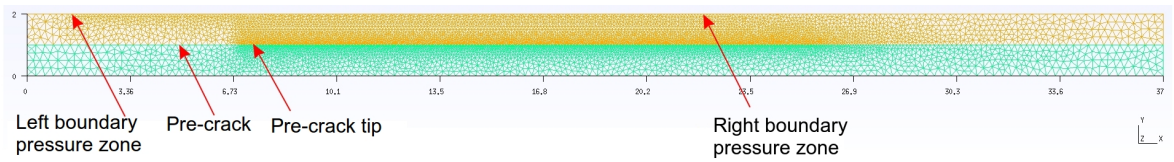

Figure 3.1: Model Mesh: upper right corner of the specimen

A notch has been applied to the model, functioning as the pre-crack, as applied to the experiment sample by the release films. Extending from the pre-crack along the full length

of the model are cohesive interface elements, used for the crack initiation and propagation.

The subsections below describe the material models used for the interface elements and shear nonlinearity and the steps of the model refinement, which were taken to reach the base model on which the parameter study of chapter 4 has been conducted. Table 3.1 gives the model dimensions of the base model, as found by the refinement.

Area	[mm]
Model thickness	2.00
Continuous plies thickness	1.00
Cut plies thickness	1.00
Left model boundary until left boundary pressure zone	2.00
Notch length (pre-crack by release film)	7.00
Pressure zone length	20.00
Right edge of pressure zone to right model boundary	15.00
Mesh density on interface	0.05
Mesh density at applied pressure boundary	0.10
Medium mesh density	0.20
Coarse mesh density	0.30

Table 3.1: Model geometry dimensions and mesh properties

3.1.1 Material model

For this study, the interface elements in the model have been fitted with the cohesive law as written by Turon et al. [7], augmented by the friction law as proposed by Alfano and Sacco [8] to account for friction during and after crack formation. These laws have been combined by van der Meer and Sluys [2] and have been proven to give good results for the simulations of the classical TCT test. In this cohesive law, the traction on the interface consists of a cracked and uncracked part, proportional to the damage variable, defined as $\mathbf{t} = (1-\omega)\mathbf{t}^u + \omega\mathbf{t}^c$. The combination of laws offers the possibility to test for the influence of friction during crack initiation and propagation, by allowing the presence of friction in partly cracked interface elements. The elastic traction of the uncracked subdomain $\mathbf{t}^u$ and cracked subdomain $\mathbf{t}^c$ are proportional to the damage variable ω, which ranges from 0 to 1, 1 being a fully formed crack. The applied parameters in the model are reported in Table 3.2, a more extensive description of the interface model can be found in ref. [2].

K [MPa]	Dummy stiffness	1.e6
μ	Friction	0.05
f_{yt} [MPa]	Tensional strength	75.00
f_{xy} [MPa]	Shear strength	75.00
G_{II} [N/mm]	Mode II fracture toughness	0.80

Table 3.2: Cohesive zone parameters

For the nonlinear response of the bulk material around the crack, the damage/plasticity model as formulated by van der Meer et al. [9] has been used for this study with the addition of a hardening modulus H, as proposed by van der Meer and Sluys [2].

$$\tau_{xz} = (1-d)G_{xz}(\gamma_{xz} - \gamma^p_{xz}) \tag{3.1}$$

$$d = \begin{cases} \frac{ln(1+C_3C_4\bar{\gamma}_{xz})}{C_4}, & \bar{\gamma}_{xz} \leq \bar{\gamma}_{xz}^{crit} \\ \frac{ln(1+C_3C_4\bar{\gamma}_{xz}^{crit})}{C_4}, & \bar{\gamma}_{xz} > \bar{\gamma}_{xz}^{crit} \end{cases} \tag{3.2}$$

$$\bar{\gamma}_{xz}^{p} = \begin{cases} \frac{ln(1+C_1C_2\bar{\gamma}_{xz}^2/2)}{C_2}, & \bar{\gamma}_{xz} \leq \bar{\gamma}_{xz}^{crit} \\ \frac{ln(1+C_1C_2(\bar{\gamma}_{xz}^{crit})^2/2)}{C_2} + (\bar{\gamma}_{xz} - \bar{\gamma}_{xz}^{crit})(1 - \frac{H}{G_{xz}(1-d)}), & \bar{\gamma}_{xz} > \bar{\gamma}_{xz}^{crit} \end{cases} \tag{3.3}$$

As shown in Eq. 3.1, the shear stress τ_{xz} is related to the shear strain γ_{xz}, with γ_{xz}^{p} the plastic shear strain, G_{xz} the initial shear stiffness and d the damage variable. Damage and plastic strain evolve according to Eq. 3.2 and Eq. 3.3. Evolution of the damage variable d also depends on the history variable $\bar{\gamma}_{xz}$, defined as the maximum history value of γ_{xz}. The conditional value $\bar{\gamma}_{xz}^{crit}$ is the lowest positive value of γ_{xz} for which $\partial\tau_{xz}/\partial\gamma_{xz}$ $= H$. The variables C_1 up to C_4 are material parameters, which are used to fit an experimental stress-strain relation for the applied material as proposed by van Paepegem et al. [10]. The appropriate parameters of the material used in the experiment are not known at the time of this study. As a realistic estimate of these parameters, the same values were used as in van der Meer and Sluys [2], which can be found in Table 3.3. This means that the comparison of the analysis results with the experimental results is done for the trends/phenomena in a qualitative manner only. More detailed information on the material models can be found in ref. [2].

G_{xz} [MPa]	5290.00
H [MPa]	3.00
C_1	25.00
C_2	-34.00
C_3	46.00
C_4	-4.00
E_x [MPa]	171420.00
E_y [MPa]	9080.00
ν_{xy}	0.32
ν_{yz}	0.40

Table 3.3: Material model parameters

3.1.2 Model length

Using symmetry while modeling reduces the computation time significantly, but with the applied element size, a horizontal model length of 100 mm still gives rise to excessive computation times. A fixed length for the pressure zone of 20 mm is applied in the experiments and therefore in the model too. A parameter study has been done on the length of the model concerning the areas left and right of the pressure zone, to find the lowest length with acceptable accuracy. Using the highest compressive stress of 102 MPa for this study has given the most distinct results. A comparison was made between the force at which the load-drop occurs in the model, to determine for which length an increase of the model size no longer influences its results.

In the area to the left of the pressure zone, the notch is present, representing the release film to simulate the pre-crack. A length of 25 mm from the cut in the discontinuous plies until the left boundary of the pressure zone, indicated by 'a' in Figure 3.2 is used in the experiment. A parameter study with lengths of 1, 2, 3, 4 and 5 mm from the left boundary

of the model to the left boundary of the pressure zone has been done to investigate its influence.

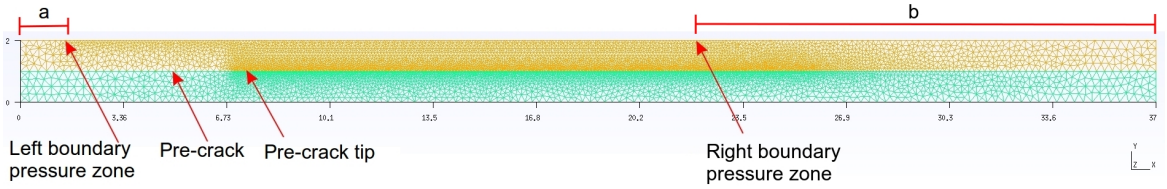

Figure 3.2: Left (a) and right (b) boundaries of pressure zone until model boundaries

Below in Figure 3.3, the load-displacement diagrams of the 5 lengths are shown. As can be seen, the length of the model left of the pressure zone has no influence on the load drop values. The difference in displacement is in accordance with the extra length of the model.

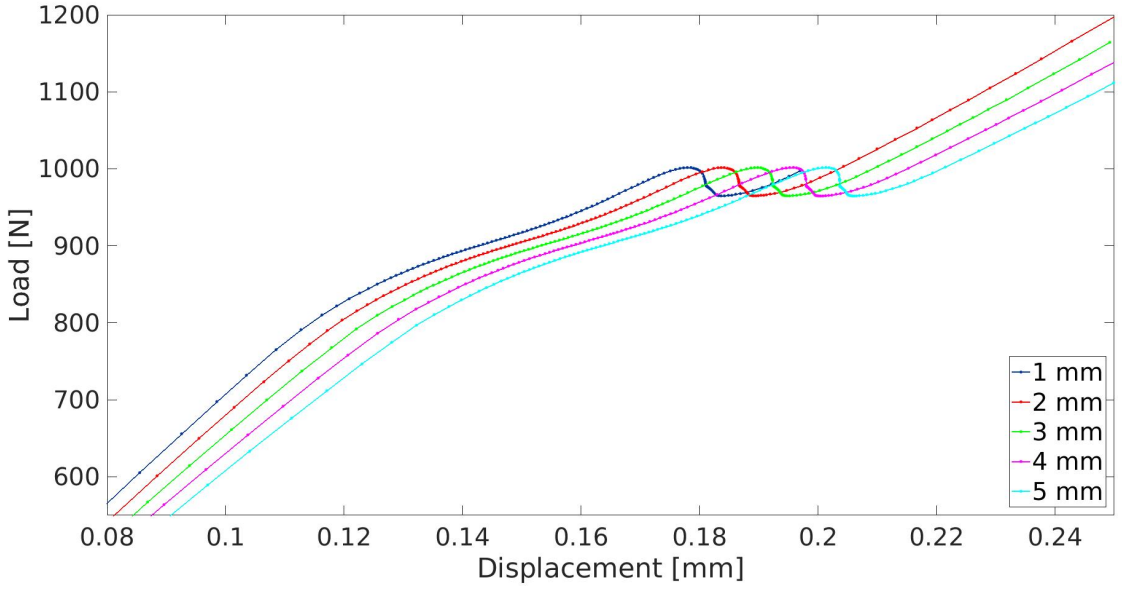

Figure 3.3: Load-displacement diagrams for lengths of the left side (a) of the model

To the right of the pressure zone, indicated by 'b' in Figure 3.2, which is 55 mm in the experiment, crack initiation and propagation is present during the loading stage. The 6 different lengths of 6, 9, 12, 15, 18 and 21 mm are applied to this part of the model. From Figure 3.4, it shows that the length of part 'b' is of influence on the severity of the load-drop, and due to this, for short lengths also on the maximum load. Increasing the length makes the drop steeper until the point at which the convergence is lost, but the maximum load is converging to a constant value. The influence of the length of the model against the maximum load is shown in Figure 3.5.

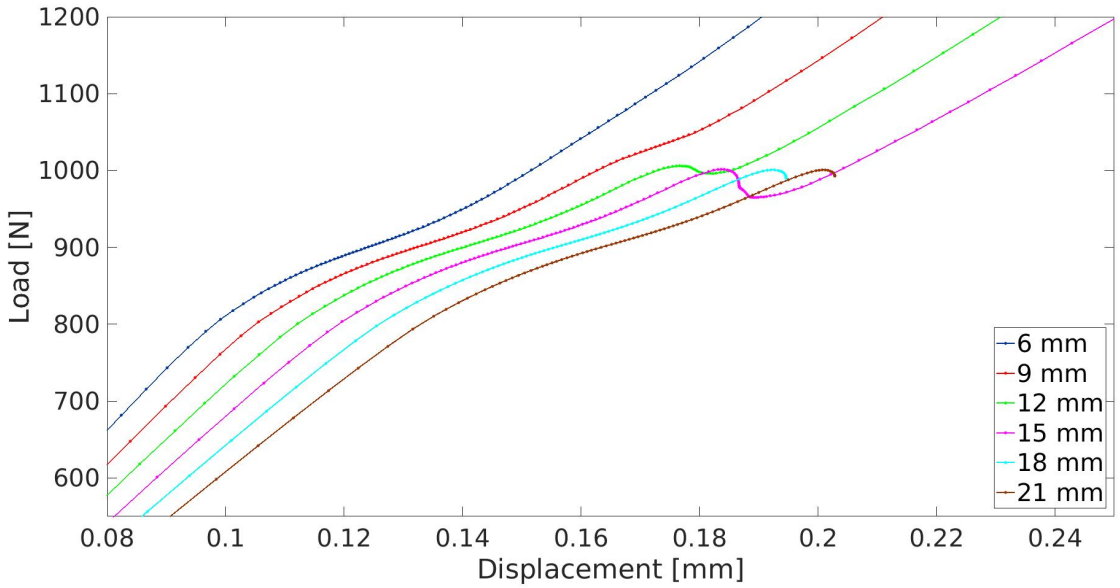

Figure 3.4: Load-displacement diagrams for lengths of the right side (b) of the model

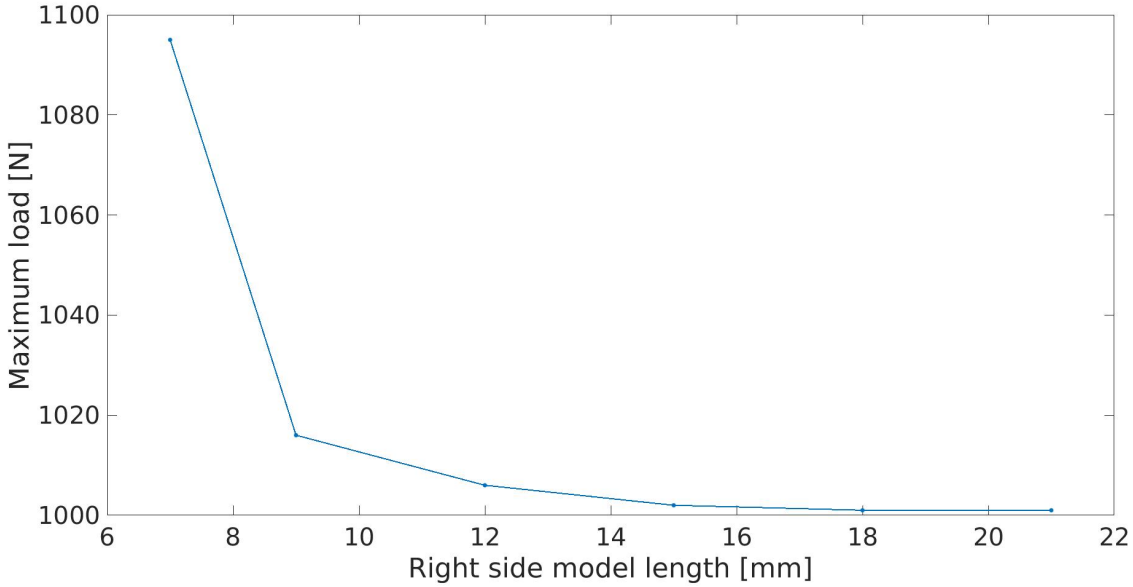

Figure 3.5: Right side (b) model length influence

From these results, the model length has been set to 37 mm for this research. A 2 mm length on the left due to its lack of influence. A 15 mm length on the right side of the pressure zone is applied, since increasing the length on the right side beyond 15 mm will lower the load drop value by only 0.1%.

Even though the length of the right side of the model influences the maximum load, the crack initiation load and start of the crack propagation load, denoted by the transition of the first (linear) into the second branch of the diagram, is unaffected.

3.1.3 Mesh refinement and dependency

A mesh refinement and dependency study is done to determine a mesh size with acceptable accuracy of the results, and to test for mesh dependency.

Varying mesh sizes have been applied over different areas of the model. The areas are identified as the area left of the pressure zone, right of the pressure zone, near the interface elements inside the pressure zone and the top and bottom boundaries of the model. After this refinement study on the areas, a minor influence on the results from the elements left of the pressure zone and the top and bottom of the model were found. A more significant influence was found from the element size of the mesh around the interface elements inside and close to the right side of the pressure zone.

The results shown below are of the study performed on the interface element size under a compressive stress of 102 MPa, in which element sizes of 0.20, 0.10, 0.05, 0.02, 0.01 and 0.005 mm have been applied. Plotting the results on a logarithmic scale against the maximum loads, identified by the maximum value for the applied load before the load drop, shows no convergence towards a constant value when using smaller elements, as can be seen in Figure 3.6.

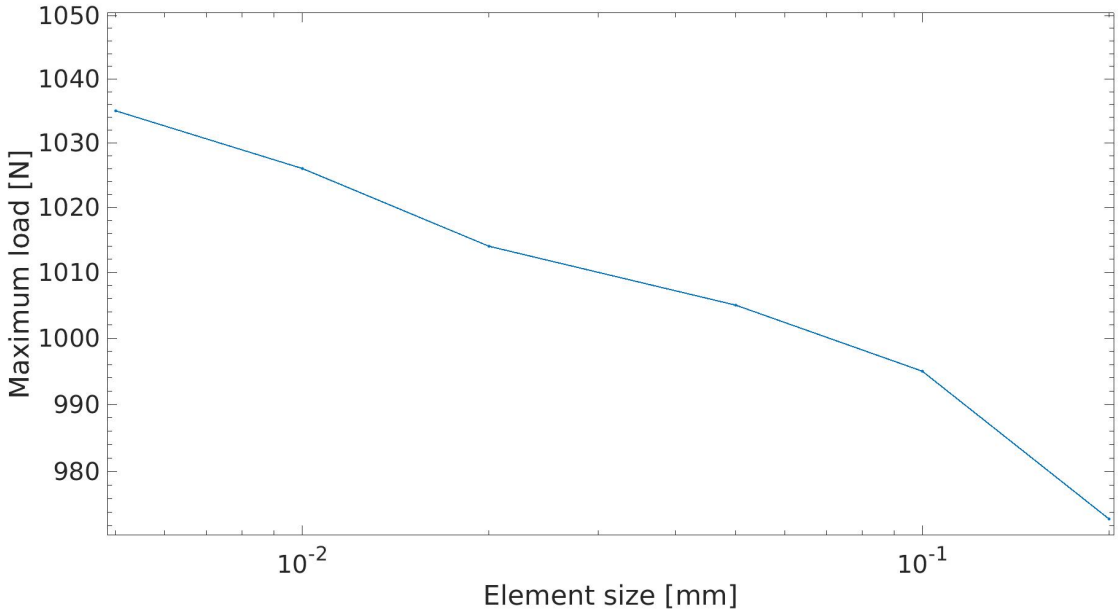

Figure 3.6: Mesh dependence

The mesh size at the top of the model in the pressure zone area has been set to 0.1 mm, to allow for clear implementation of the compressive stresses, done by point loads per node. In the interface area, an element size of 0.05 mm has been applied as the most refined region, giving an acceptable duration of the calculations. This mesh size is applied past the right boundary of the pressure zone into 'b' (Figure 3.2) for 3.5 mm, after which the element size no longer influences the results. The other areas of the model have been given a medium and coarse mesh density as specified in Table 3.1.

For the test with the smallest element size of 0.005 mm for the cohesive zone, there is still mesh dependence. This is in accordance with van der Meer and Sluys [2], where the smallest applied element size of 0.003 mm and a hardening parameter H of 3, still shows mesh dependence. This dependency was found to be caused by the damage/plasticity model described in section 3.1.1, applied to the bulk material. Shear stress concentrations around the crack tip cause plastic deformations, which is a very local phenomenon and sensitive to the element size. Decreasing the element size is expected to lead to mesh independent behavior of the bulk material around the crack tip.

Chapter 4

Parameter study

A parameter study is done to determine the influences of the chosen variables on the results of the model output. This chapter gives a description of the basis model without compressive stress for reference, and the results of the parameter study. It also links the experimental results to the model results for validation, closing the section with a summary of the characteristics of the model as found by the parameter study.

4.1 Basis model characteristics

A calculation of the model with a through the thickness compressive stress of 0 MPa, which can be used as control model and for comparison was performed, similarly to the control data used in the experiment of Catalanotti et al. [5]. Shown in Figure 4.1 is a linear branch until crack initiation, followed by crack propagation at a constant load, until the crack has reached the right boundary of the model and a linear branch follows for the continuous plies in tension similar to results in ref. [2].

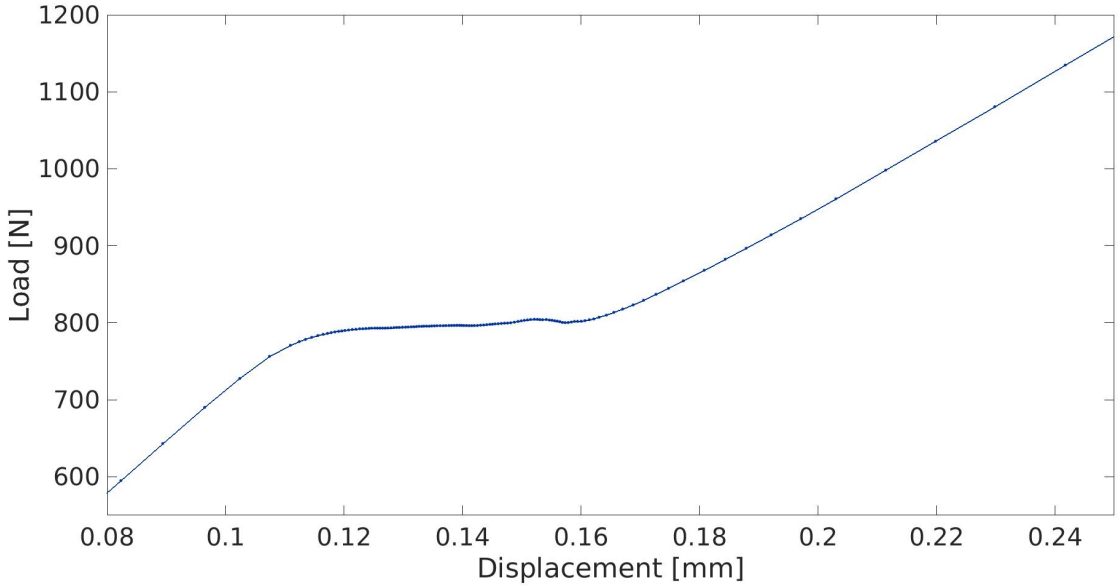

Figure 4.1: No compressive stress basis model

As the basis model represents a standard mTCT test, the analytical formula for the fracture toughness as in Eq. 2.1 applies. This complies with the test results, as there is crack propagation for a constant load until failure, giving a constant fracture toughness from Eq. 2.1. As a result of this, the maximum load can be used to calculate the fracture

toughness.

4.2 Parameter study

In the used model, the different variables which influence the results are; the input value of the mode II fracture toughness, the shear strength of the material, the length of the pressure zone, the compressive stress applied to the model and the friction coefficient. The effects of different values for these parameters are shown in the following sections.

4.2.1 Fracture toughness

The finite element model requires an input value for the fracture toughness of the material and simultaneously delivers values that are used to compute this fracture toughness. In the analysis, the input fracture toughness is defined as the total amount of energy dissipated during crack growth in an interface element, in the absence of friction. This is also schematised as the area below the graph in Figure 2.1, denoting the fracture toughness per cohesive element.

In this section, the input values for the fracture toughness are plotted against the load displacement results and the maximum load value before the load drop. The applied values for the fracture toughness are 0.6, 0.7, 0.8, 0.9 and 1.0 N/mm, with a compressive stress of 102 MPa.

As shown in the results below in Figure 4.2, increasing the fracture toughness increases the value at which the crack starts to propagate and fail. The crack propagation has a linearly increasing branch in the load displacement diagram, which increases at the same rate for each fracture toughness.

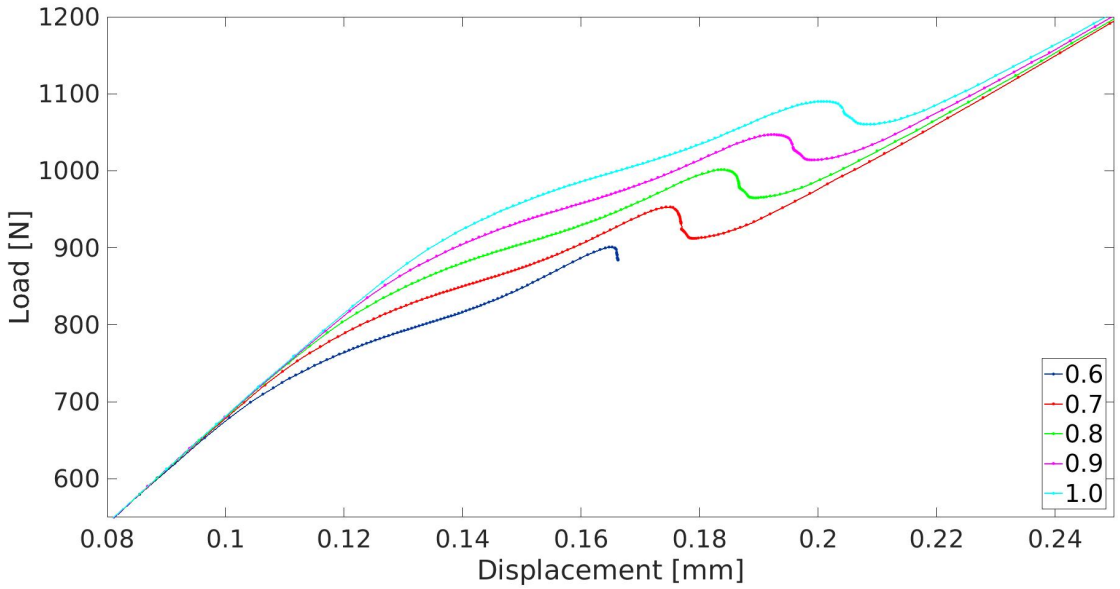

Figure 4.2: Load-displacement diagrams for varying fracture toughness

When comparing the initiation of the crack growth and the maximum load before the load-drop to the input fracture toughness in Figure 4.3, both values increase by the same, nearly linear rate. Eq. 2.1 can be rewritten to give Eq. 4.1, which gives the tensile stress of the specimen at which crack propagation occurs until failure in a standard mTCT test. This value is added to Figure 4.3 to compare to the crack initiation load of the model, as

friction during crack formation in the first elements has minor influence on the total load on the specimen.

$$\sigma = \sqrt{\frac{G_{II}}{\frac{H}{2E_1}(\frac{1}{\xi})}} \tag{4.1}$$

Using the fitted empirical parameter $\eta = 0.0035$ from Catalanotti et al. [5], Eq. 4.2 is added to Figure 4.3 to compare to the maximum load.

$$\sigma = \sqrt{\frac{G_{II} * 1.357}{\frac{H}{2E_1}(\frac{1}{\xi})}} \tag{4.2}$$

Comparing both the crack initiation and maximum loads from the analytical approaches to the model results shows underestimated values for both phenomena.

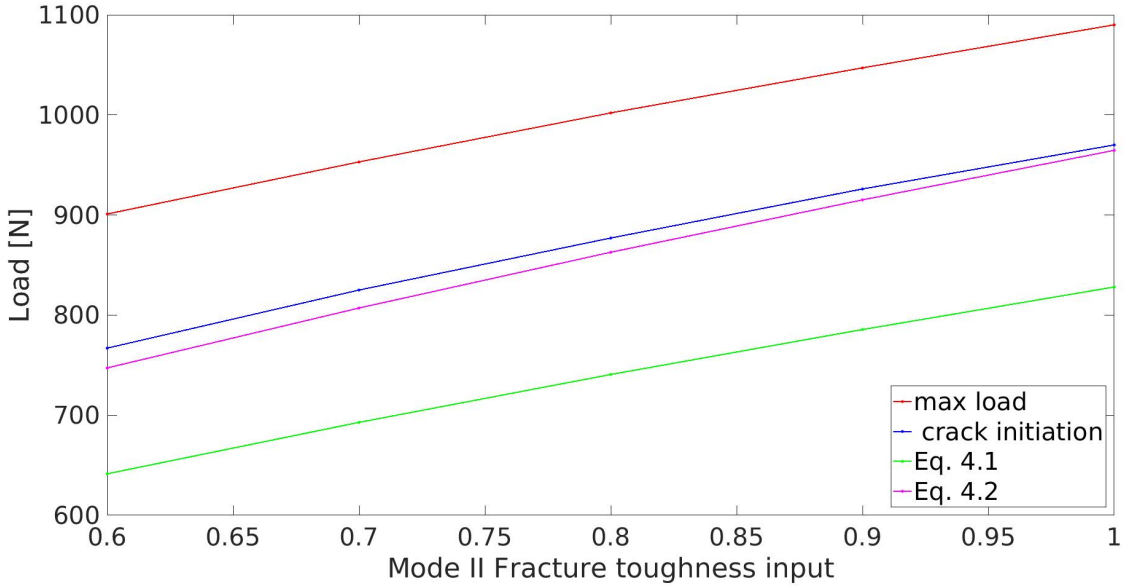

Figure 4.3: Initiation and maximum load for mode II fracture toughness

Using Eq. 4.1 and 4.2 for the calculation of the mode II fracture toughness, the input value is compared to the output values for the initiation load and the max load in Table 4.1. With every 0.1 increase in the input value, the output value for the initiation load increases by 0.13 and for the max load by 0.14.

Input G_{II} [N/mm]	Initiation load (Eq. 4.1) G_{II} [N/mm]	Max load(Eq. 4.2) G_{II} [N/mm]
0.6	0.86	1.18
0.7	0.99	1.32
0.8	1.12	1.46
0.9	1.25	1.60
1.0	1.37	1.73

Table 4.1: Input and output fracture toughness

To find the traction exerted by the interface elements in the x-direction, the force from the elements is augmented with the friction, resulting in the traction as shown in

Figure 4.4. The red and blue lines represent the force during the formation of damage in the interface elements. The diagram indicates the position of the crack formation in the model and the traction at the given location by the interface elements. An interval of 5 timesteps has been used for clarity. Indicated by the red lines is the model with a mode II fracture toughness of 1.0, the blue lines of that with 0.6. A lower fracture toughness input results in a steeper diagram.

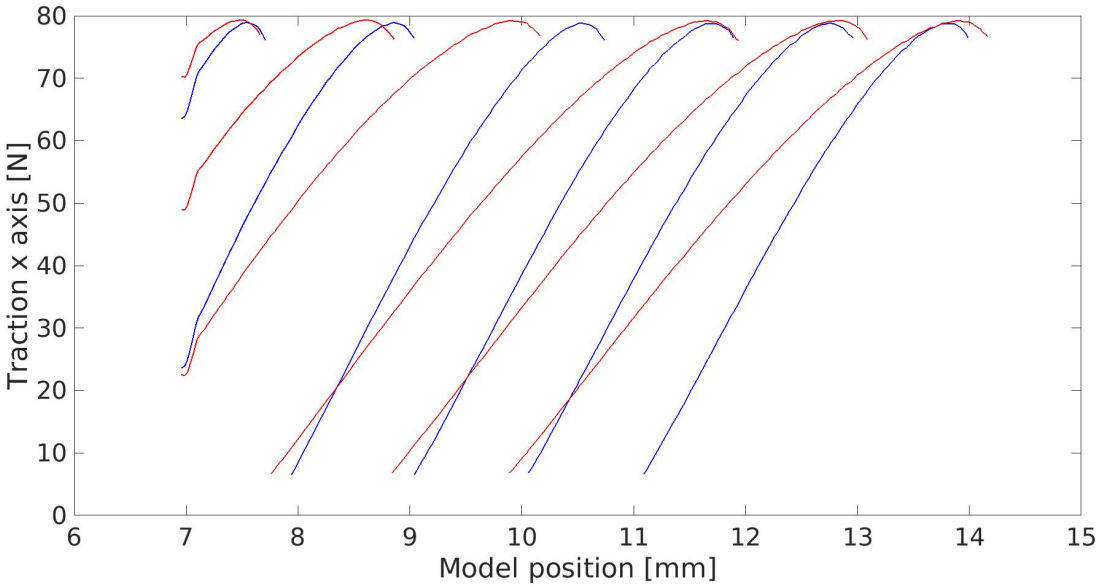

Figure 4.4: Traction in x-direction in the interface elements

Increasing the input fracture toughness of the model results in an equally increasing load value for the start of crack propagation and for the maximum load. If the area of the constitutive relation for the fracture energy as in Figure 2.1 increases without an increase in shear strength, the second branch becomes less steep, increasing the maximum strain per interface element. With the friction added to this, the traction in the x-direction, exerted by the interface elements as plotted in Figure 4.4 increases at a lower pace. The maximum traction remains equal due to the friction as well as the maximum shear force for the interface elements being unchanged. Damage formation requires larger strains, resulting in more interface elements participating in the total traction exerted in the model, which leads to an increase in failure and crack growth initiation load.

As can be seen in Table 4.1, the input values do not match the values calculated from the output of the model. A linear increase of the input value gives a linear increase of the output values, but not of the same magnitude.

Comparing Figure 4.3 to the basis model of Figure 4.1, crack initiation for $G_{II} = 0.8$ occurs around the same load, but crack growth appears in a load range instead of a constant value.

4.2.2 Shear strength

As a model parameter, the shear strength is of influence on the results. This section shows the results of various values of the shear strength applied in the model.

A standard TCT fracture toughness test uses the analytical approach with the failure stress and sample thickness as input. The shear strength does not affect these results, but due to interaction with the damage/plasticity model, it does have an influence on the model results. First, for a compressive stress of 0 Mpa, varying shear strengths have been applied to the model with and without shear damage.

Figure 4.5 compares the load displacement diagrams for the shear strengths of 45 MPa until 95 MPa, with shear damage and 0 MPa compressive stress applied in the model. A constant load for crack growth, but an increase in the crack initiation and failure load is found for higher shear strengths. The crack growth load does not increase by the same magnitude as the shear strength.

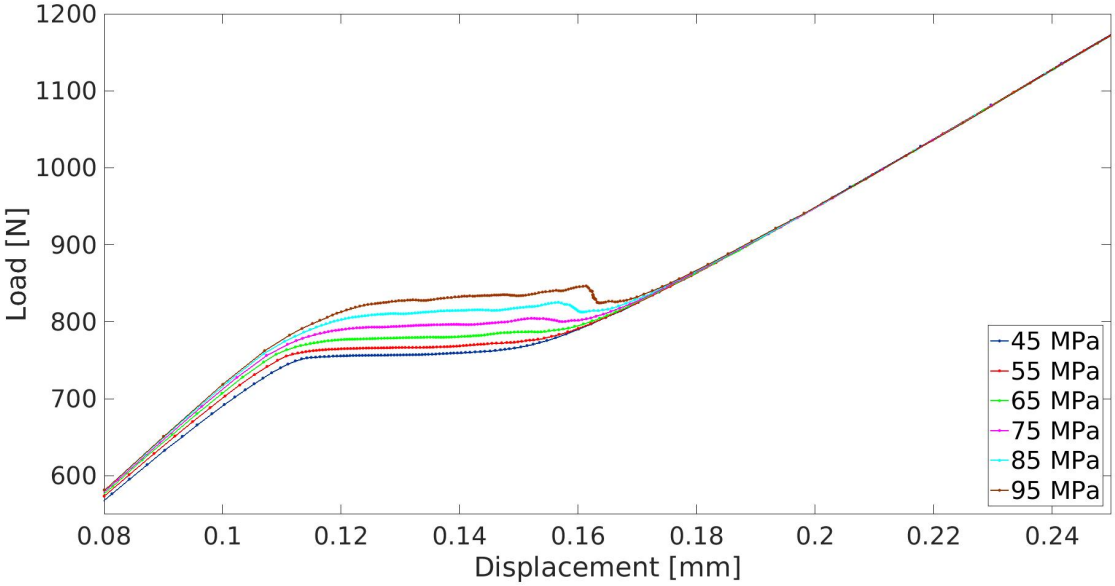

Figure 4.5: Load displacement diagrams of varying shear strength with shear damage under 0 MPa compressive stress

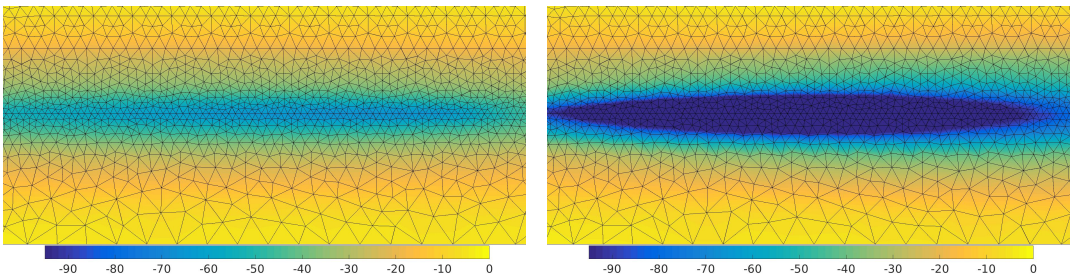

Figure 4.6: Shear stress τ_{xy} at 45 MPa (left) and 95 MPa (right) shear strength

Compared in Figure 4.7 are both load displacement diagrams without shear damage. The crack growth load is again constant for both shear strengths, but apart from a sharper transition from the linear branch to crack growth for the higher shear strength, both diagrams give the same results.

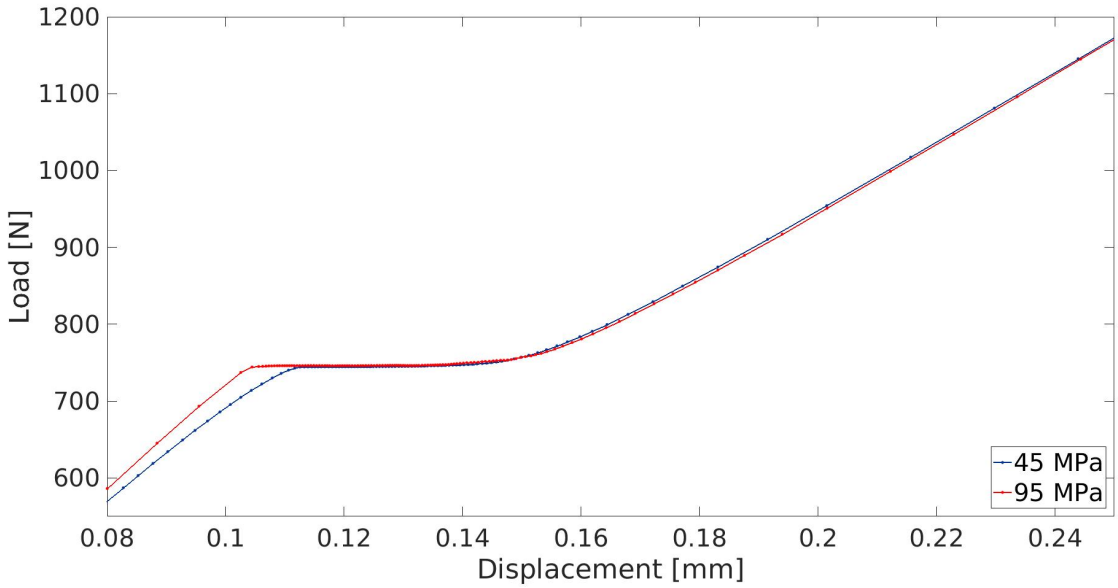

Figure 4.7: Load displacement diagrams of varying shear strength without shear damage

For both compressive stresses of 17 MPa and 102 MPa, the shear strength values of 45, 55, 65, 75, 85 and 95 MPa are tested, with shear damage applied, to see the influence of the complete model.

A higher shear strength gives an increase in the crack growth load in the model, for an applied compressive stress of 17 MPa, but this load does not increase with the same magnitude as the increase of the shear strength as seen from Figure 4.8, in accordance with Figure 4.5.

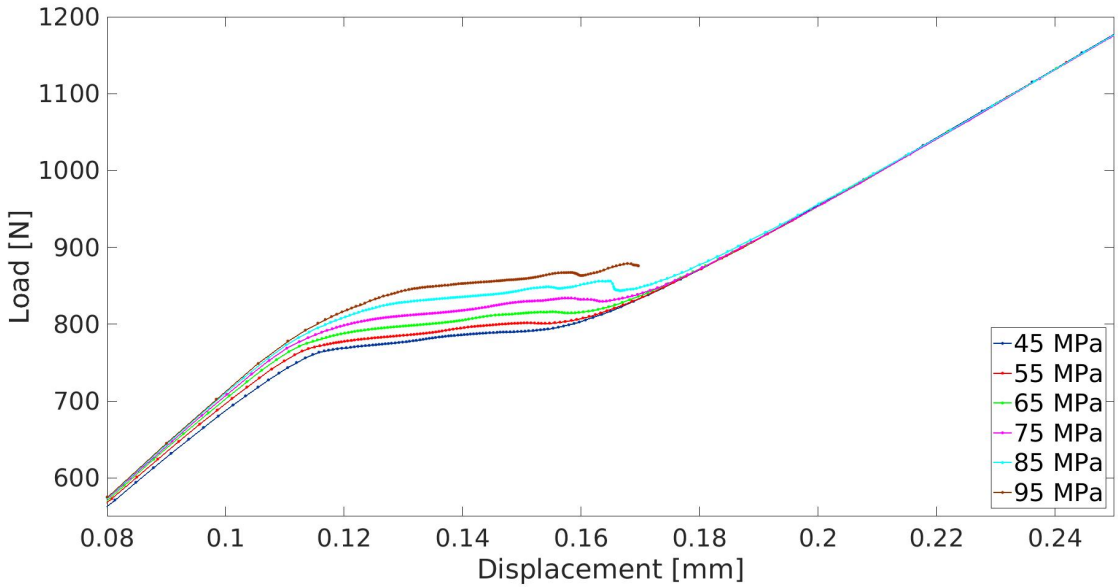

Figure 4.8: Load displacement diagrams of varying shear strength at 17 MPa compressive stress

When all load displacement diagrams for the compared shear strengths under a compressive stress of 102 MPa are plotted as below in Figure 4.9, the results are similar to Figure 4.8. The main difference lies in the range of the crack growth values, which are larger for the higher compressive stress.

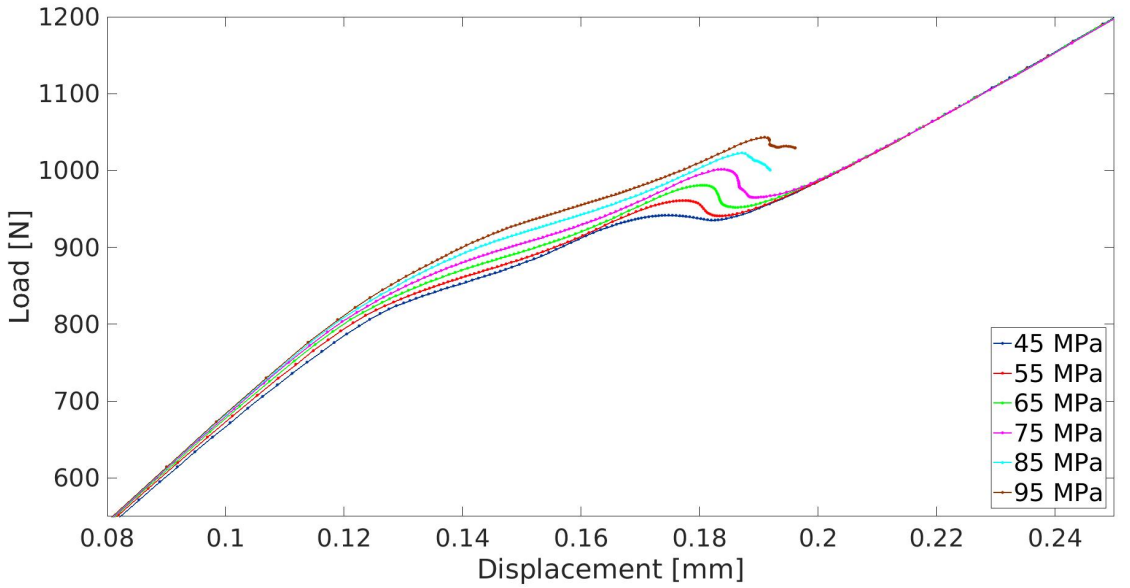

Figure 4.9: Load displacement diagrams of varying shear strength at 102 MPa compressive stress

For the compressive stress of 17 MPa, lower maximum loads are found than for 102 MPa, but as shown in Figure 4.10, there is an increasing relation between the shear stress and the maximum load. For the case of 102 MPa compressive stress, a nearly linear relation is found for the maximum loads.

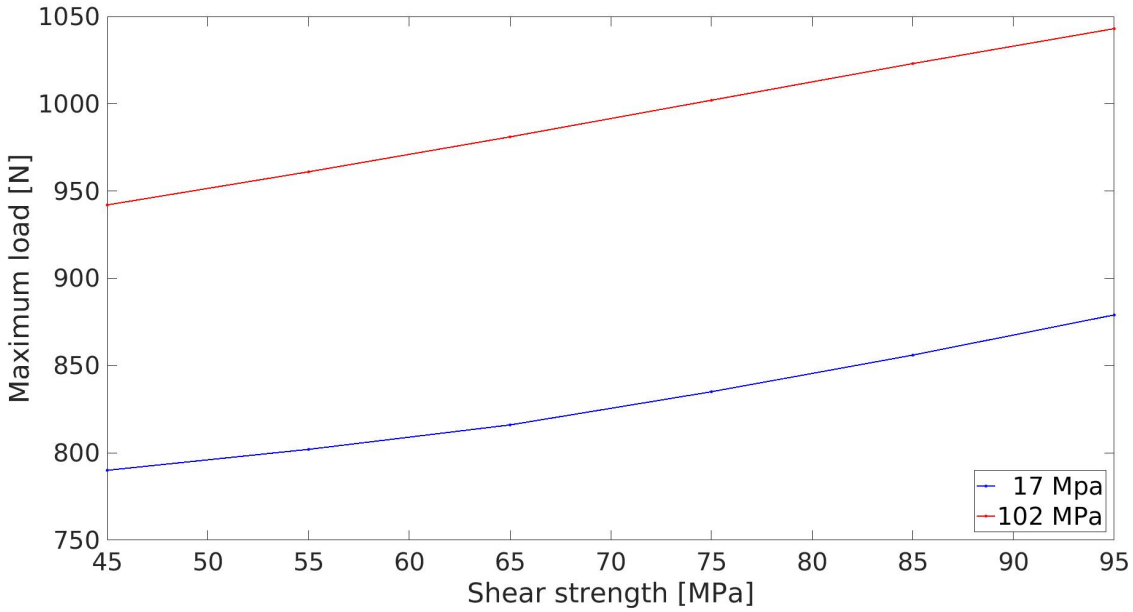

Figure 4.10: Maximum loads for varying shear strength under 17 and 102 MPa compressive stress

Because the purpose of this test is the measurement of fracture energy, energy dissipation mechanisms are a key element in this numerical study. From the investigated parameters, the shear strength is the only mechanism which does not influence the energy dissipation directly. The influence of it on the plasticity of the model, which is an energy dissipation method, gives the motivation to include the shear strength in the parameter study.

Comparing Figure 4.5 to 4.7 shows which part of the model is influenced by a variation in shear strength. The damage/plasticity model from Eq. 3.1-3.3 will reach its elastoplastic region in the elements around the crack tip before the interface elements will reach the maximum shear stress. This allows the load to increase further for a higher shear strength as can be seen from Figure 4.6. A higher shear stress is reached around the crack, resulting in an increased crack growth load. The exponential increase in crack growth load, for a linearly increasing shear strength, likely follows from a larger elastoplastic region around the crack tip for a higher shear strength.

When damage/plasticity is not applied to the model, the crack growth load for both shear strengths is equal, as expected. The influence on the transition to crack growth is caused by the second branch of Figure 2.1, which will have a steeper decrease when the shear strength is increased.

Increasing the shear strength has nearly the same effect for both compressive stresses on the model. The main difference in results for the varying shear strengths under different compressive stresses is an increase in the range of the crack growth load.

4.2.3 Pressure zone length

A variation in the length of the pressure zone is an external parameter, unrelated to the sample material. Because it is related to the compressive stress, the influence of the length on the results are studied and reported in this section. A compressive stress of 102 MPa has been applied for the calculations due to its higher influence compared to a lower compressive stress.

The length of the pressure zone has been varied from 18 mm up to 28 mm, while the length of the model left and right of the pressure zone has been kept constant. To compare the influence of the length in combination with the compression, the length of 18 mm and 28 mm have first been compared without compressive stress. Figure 4.11 shows a constant crack growth load, but an increase in the strain at which the crack starts to propagate for a larger pressure zone. The same effect happens for the displacement at failure, except that the model with 28 mm pressure zone has a larger total displacement for the crack growth branch than the shorter model.

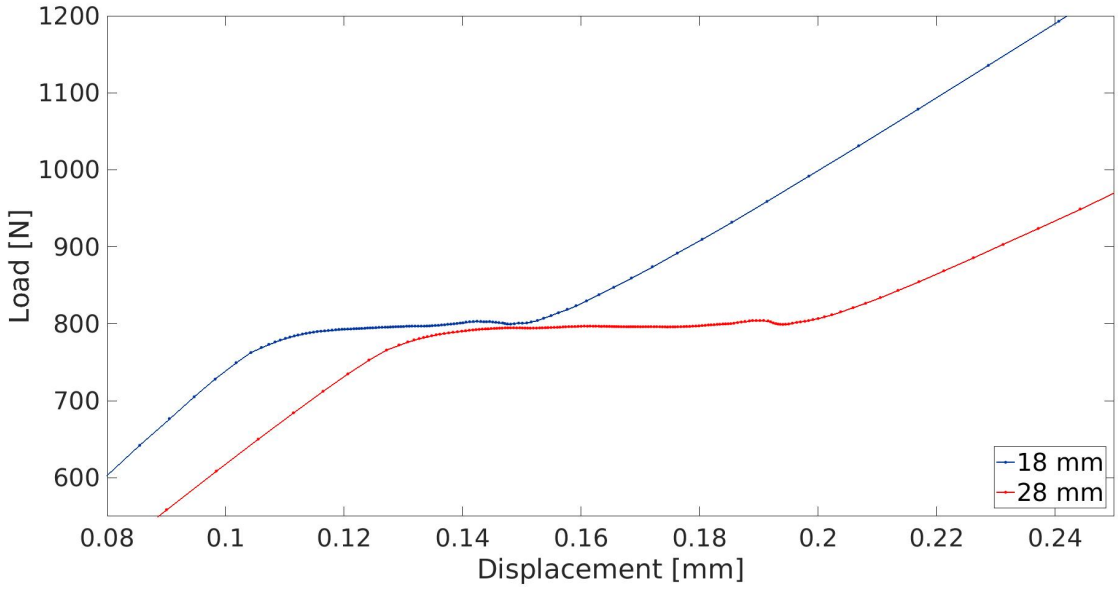

Figure 4.11: Load displacement diagrams at 0 MPa compressive stress

Crack growth initiation for all lengths of the model under compressive stress occurs

at the same load, as can be seen from Figure 4.12. Comparable to Figure 4.11, the displacement at the maximum load increases more than the crack growth initiation for larger pressure zones, resulting in a higher maximum load.

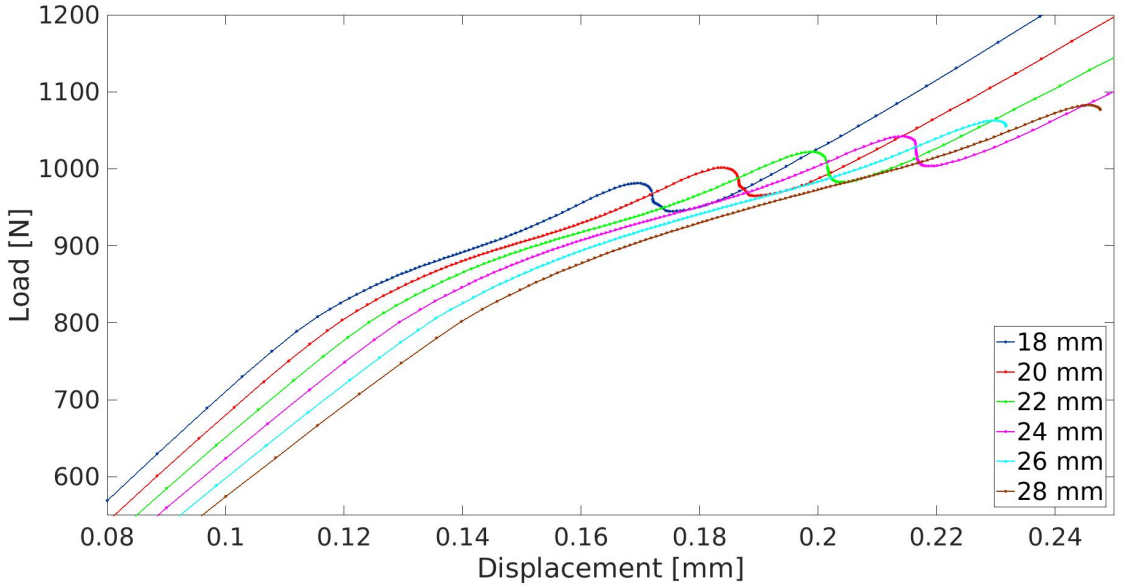

Figure 4.12: Load displacement diagrams for varying pressure zone lengths

When plotting the failure loads from Figure 4.12 against the lengths of the pressure zone in Figure 4.13, a linear relation is found.

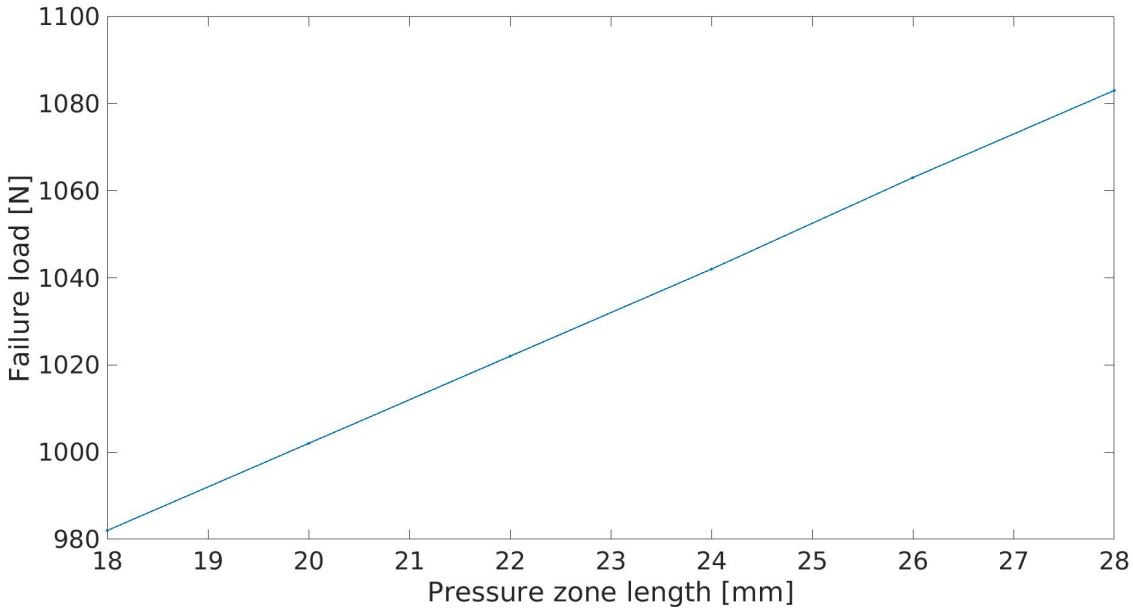

Figure 4.13: Maximum load for varying length of the pressure zone

Increasing the length of the pressure zone has a consistent influence on the results of the model. Figure 4.12 shows a constant crack initiation load and a linear increase in failure load for an increasing length of the pressure zone. Comparing this to Figure 3.3, shows that increasing the length of the model inisde of the pressure zone has a clear influence on the failure load, where an increase outside of it does not.

Even though the influence of the length of the pressure zone is clear from the results,

it is not a parameter in the analytical formulation of the mode II fracture toughness as in equation 2.1 and 2.2. Applying the tensile stress in the specimen at the moment of failure will result in a different fracture toughness, depending on the length of the pressure zone.

4.2.4 Compressive stress

With increasing through the thickness compressive stress, the apparent fracture toughness has been seen to increase too. This section reports the influence of the compressive stress applied in the model, on the crack propagation.

All compressive stresses are applied in the model as described in section 2.2, as well as the control setup with $\sigma_{33} = 0$ MPa. Plotted in Figure 4.14 are all load displacement diagrams, which show an increase in the load required for crack propagation, for an increasing compressive stress.

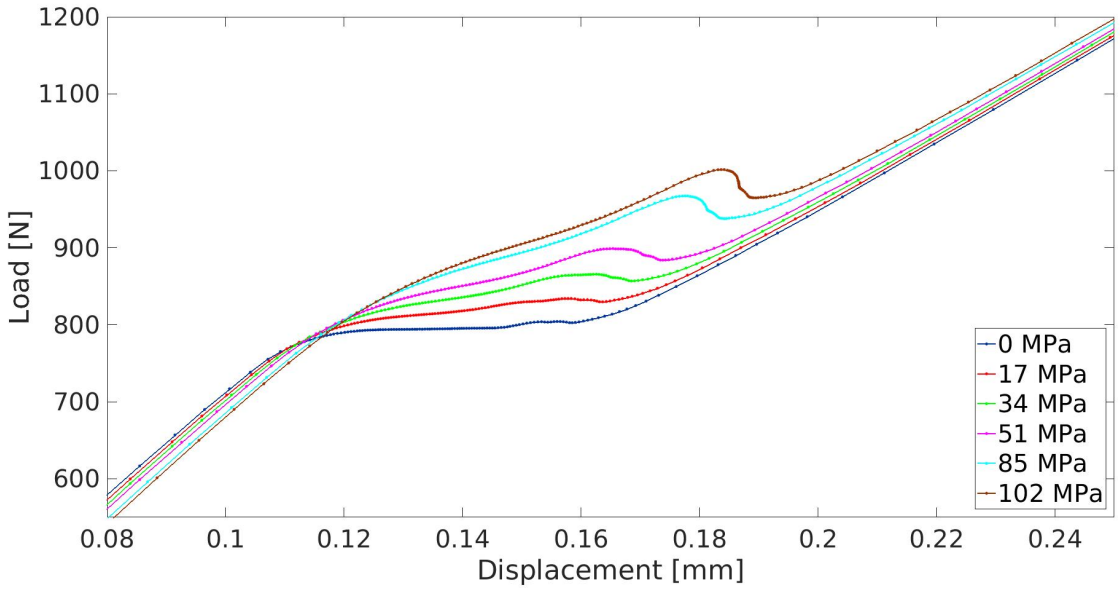

Figure 4.14: Load displacement diagrams for all compressive stresses

After the first bend in the load displacement diagrams, crack propagation is found during the second nearly linear part of the graphs. The 'start of propagation' values related to this are plotted in Figure 4.15. These values are found as the first step in the second linear branch of the diagram after the transition. A linear relation is found between the start of the crack propagation and the compressive stresses. The maximum load before the load drop for the chosen compressive stresses are also plotted in Figure 4.15, finding another linear relation, although steeper than the one for the start of the crack propagation.

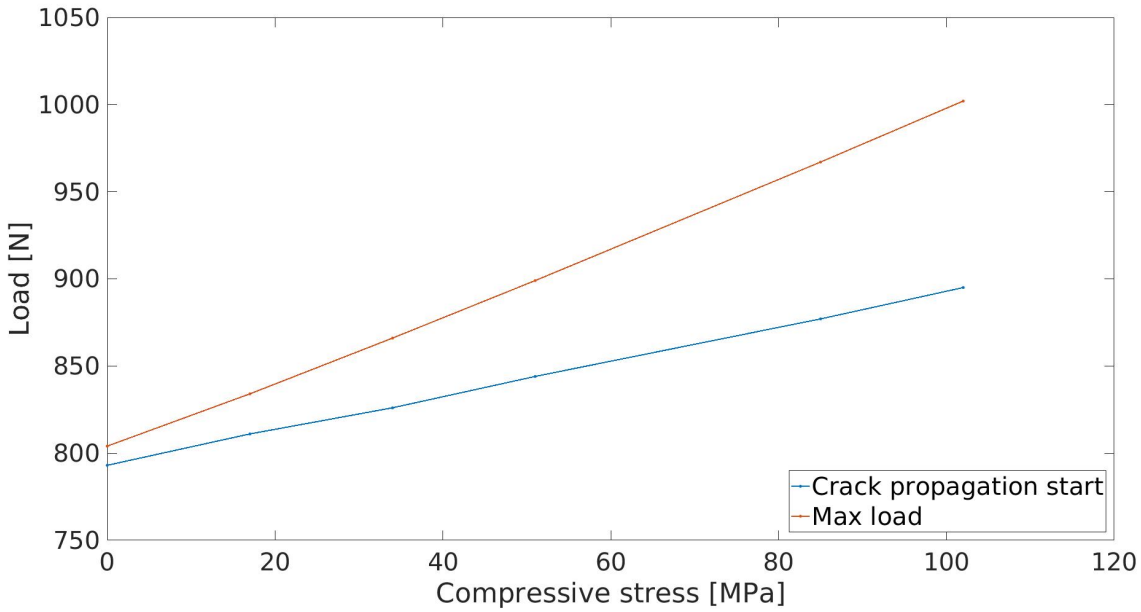

Figure 4.15: Crack propagation start and max loads for varied compressive stresses

When a through the thickness compressive stress is applied to the model, both the increase in force for the start of the crack propagation and the maximum load can be explained by friction in the model. Due to the presence of friction in the material model, a higher traction force is exerted under a higher compressive stress due to higher friction forces as soon as damage occurs. Summation of this higher traction force and the fracture energy results in a higher load at which crack propagation starts, for higher compressive stresses.

A stronger increase in maximum loads is found compared to the increase in start of the crack propagation loads, due to higher traction forces per unit of length of the propagated crack.

4.2.5 Friction

Internal friction is integrated into the continuum damage model, adding traction to the cracked area in the form of friction, from the first step at which damage occurs. As the crack propagates through the model, a larger friction area forms, increasing this force.

Due to the relation between the compressive stress and the friction, this part of the study is done under a compressive stress of 102 MPa, where the friction coefficient in the model has been varied from 0 to 0.05. The results of these tests are shown in this section, as well as the results from all compressive stresses with a friction coefficient of 0.

Comparing the output of all different friction coefficients as shown in Figure 4.16, a linear increase in the maximum load is found. In the results for the case of a friction coefficient of 0, a small load drop after crack initiation can be seen.

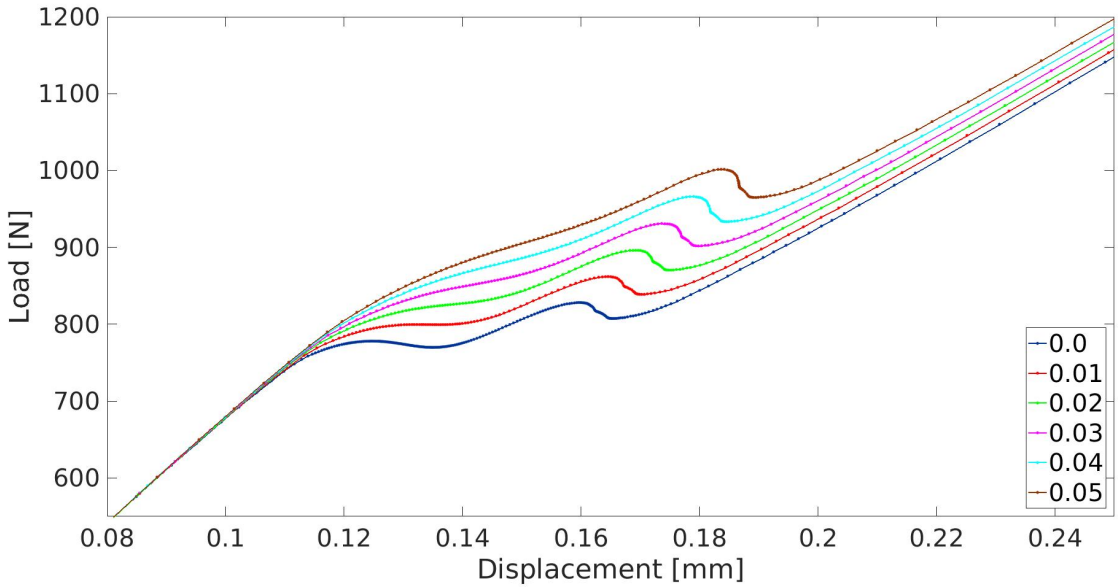

Figure 4.16: Load displacement diagrams for increasing friction coefficients

In Figure 4.17, the results of a friction coefficient of 0 in the model have been plotted. Increasing the compressive stress in this situation appears to have an influence on the crack propagation load as wel as the maximum load. For higher compressive stresses, a load drop appears after crack propagation has started, and an increase in maximum load arises when the crack reaches the end of the pressure zone.

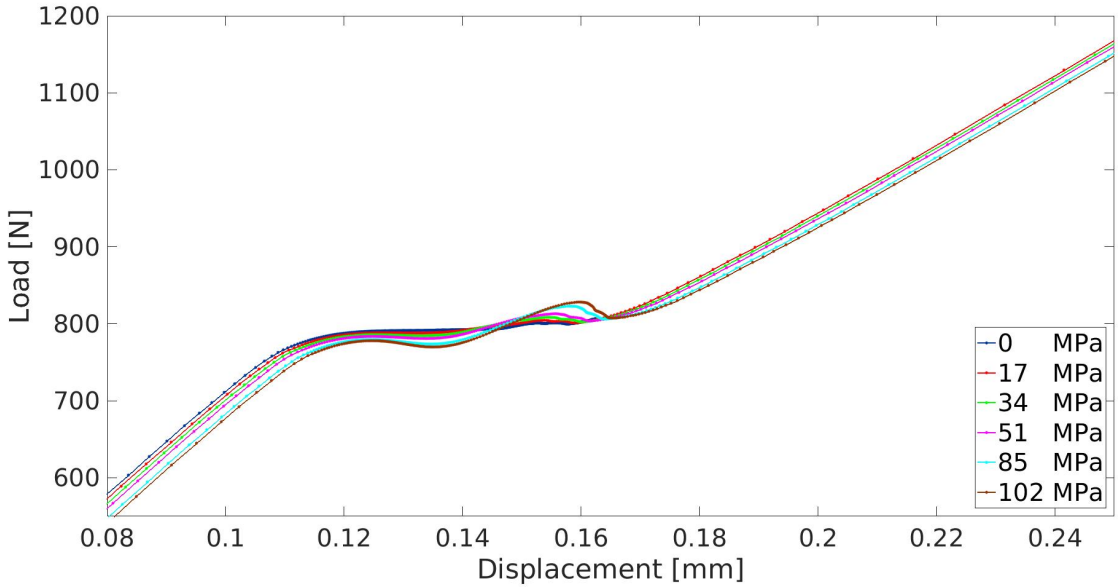

Figure 4.17: Load displacement diagrams for all tested compressive stresses at zero friction

As the internal friction coefficient increases linearly, the results of starting crack propagation load and the maximum load increase linearly too. This coincides with the constant length of the pressure zone and the increase in traction due to the friction coefficient. A similar relation was found for an increase in compressive stress and pressure zone length.

When the friction coefficient is set to zero, a load drop occurs after the start of the crack propagation and also an increase of the maximum load, for the higher compressive stresses. Further analyses showed that the young's modulus in the x_3 direction, parallel to the compressive stress, shows the same influence on the results as can be seen in Figure

4.18. This gives reason to believe that the deformation in the x_3 direction due to the compressive forces influences the results by causing a shear stress to be present near the interface.

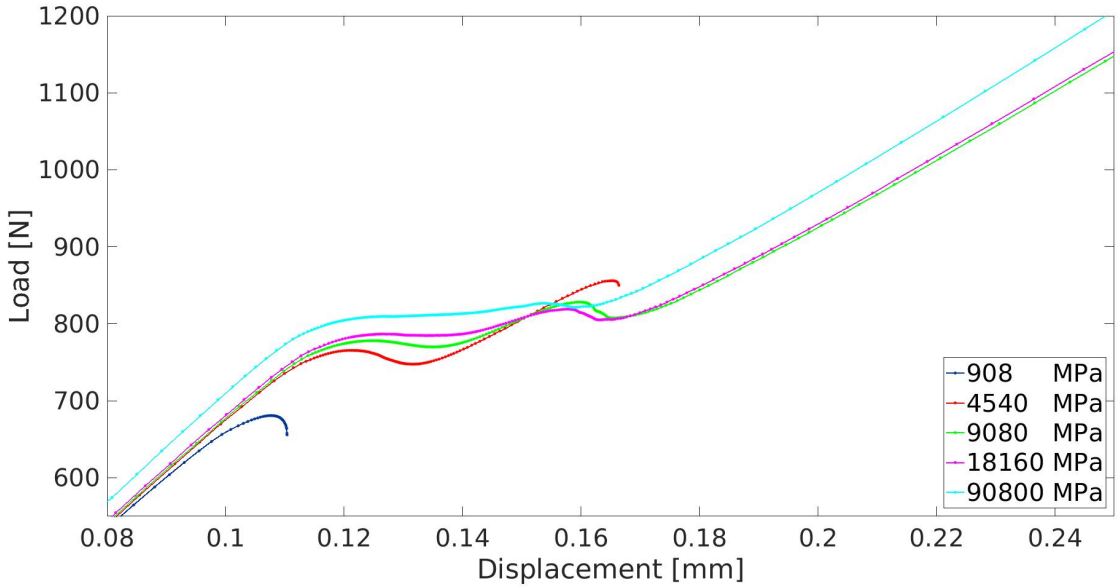

Figure 4.18: Load displacement diagrams for varying young's modulus in the x_3 direction

4.3 Matching model and experiment data

Apart from the detailed workings of the proposed model, discussed in the sections above, there should also be a link to the experimental results from [5], as shown in section 2.3. Even though a quantitative comparison of the load displacement diagrams of the experiment to those of the model can not be made due to the absence of the material parameters C_1-C_4, in a qualitative comparison can be seen that the experimental results can be linked to the model results.

Performing a computation with 102 MPa compressive stress when using the full length of the modeled part of the specimen, 100 mm, gives Figure 4.19. An apparent linear branch until failure can be seen, with a small deviation around the start of crack propagation.

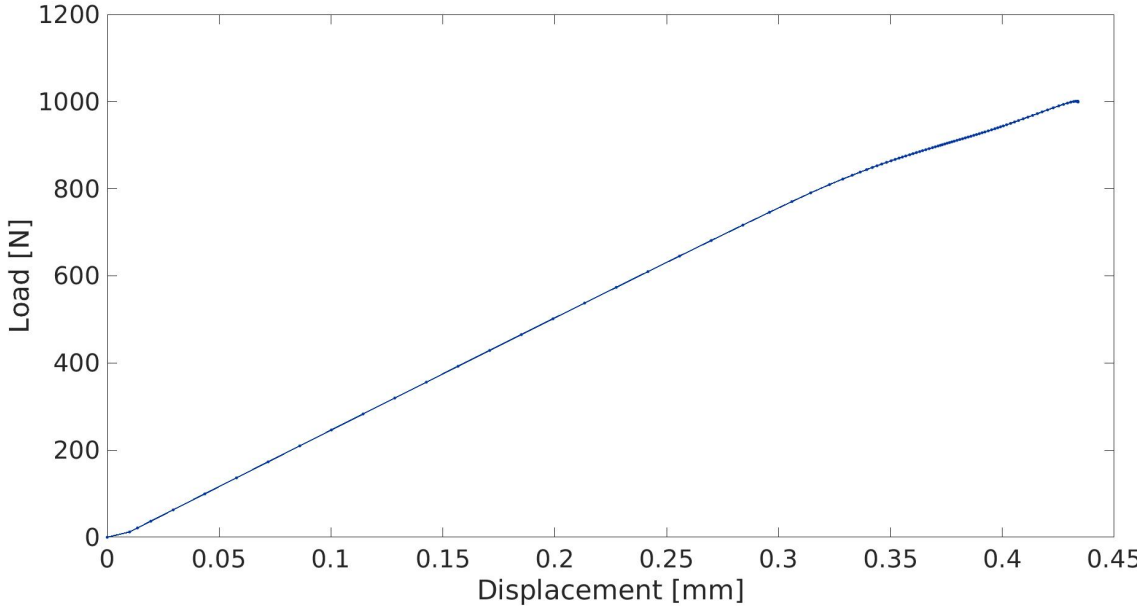

Figure 4.19: Full length (100 mm) of top right quarter of the specimen modeled

A linear loading branch until the load drop in the experimental results as seen in Figure 4.20, matches that of the model results in Figure 4.19 in a general way. The more detailed phenomena as seen in the sections above are less visible in both the model and the experimental results. The distinct second branch in all the results of the parameter study is not visibly present when modeling the full length of the specimen. This is caused by the increased length which results in a linear load displacement of the model outside the pressure zone during crack growth, partially hiding the crack growth part of the diagram.

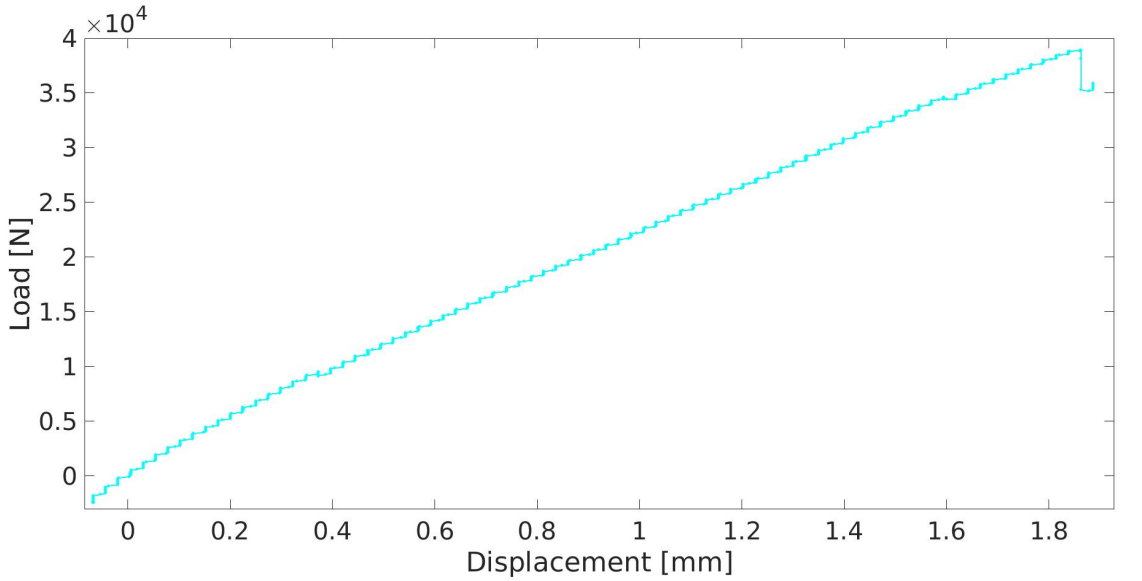

Figure 4.20: Experimental results for 102 MPa compressive stress

In most of the experimental results, those with compressive stresses higher than 17 MPa, a small displacement jump can be seen in the diagram. Figure 2.9 shows the diagrams of the tested samples for 17, 34, 85 and 102 MPa compressive stress with matching arrows at the displacement jumps. These jumps arise around the same load at which the load drop is observed for the sample with 17 MPa applied compressive stress. This displacement

jump is believed to resemble the start of the crack propagation of the model results, after which the linear branch until the load drop resembles the crack propagation until failure. This same deviation is found in Figure 4.19.

4.4 Important model characteristics

Based on the results of the parameter study, the characteristic behavior of the model is described in this section. The five different parameters that were studied, all have different effects on the output, but not all are independent from each other.

The input fracture toughness in the material model gives a higher load at which crack propagation starts and at which the maximum load will be reached for a higher input value. This effect is a nearly linear relation between the fracture toughness and both loads.

The shear strength of the material has two influences on the results. An increase in shear strength results in a sharper transition from the linear branch into the crack growth branch of the load displacement diagram. The combination with the damage/plasticity model of the bulk material results in a larger area of plastic deformation around the crack tip, this increases the crack growth load and the maximum load by the same magnitude for each increasing shear strength.

The length of the pressure zone has a linear relation to the strain at which crack propagation starts, at which the maximum load occurs and to the magnitude of the maximum load. The increase in strain at the start of crack growth is smaller than for the maximum load, when a longer pressure zone is applied. Increasing the pressure zone length does not influence the load at which crack propagation starts but does increase the maximum load, by creating a larger crack growth range.

The magnitude of the compressive stress applied to the model influences the load at the start of crack growth and the maximum load. A higher compressive stress creates a larger traction force in the interface elements as soon as damage forms. This increases the load at which the first element is fully cracked, after which crack growth occurs. As the force increases per damaged element, a higher load will occur as the crack propagates through the pressure zone, resulting in a higher maximum load for a higher compressive stress.

The friction coefficient influences the model in the same manner as the compressive stress does, due to their direct relation. For an increasing friction coefficient, a larger traction force will be exerted on the interface of damaged elements. This results in a higher crack growth initiation load and an increasing load until failure as the crack grows through the pressure zone.

A very direct relation between the pressure zone length, the compressive stress and the friction coefficient is found here. As soon as damage forms in the interface elements, the load increases per unit of length, based on the compressive stress and the friction coefficient. An increase in either of these parameters results in an increase in crack growth load range.

Chapter 5

Discussion and conclusions

5.1 Conclusions

In this section, a discussion of the results is made, followed by a general conclusion of this study. Recommendations for further research on this subject are pointed out to verify and work out still missing information.

5.1.1 Discussion and conlusions

Based on the results of this study as they are presented in this report, some implications are discussed here.

Previous research has shown a dependency of the fracture toughness on the thickness of a specimen in a TCT test, contradicting the assumption that it is a material parameter. Based on this report and the experimental results from Catalanotti et al. [5], it can be concluded that the apparent fracture toughness depends on the thickness as well as the compressive stress. In the case of the standardized test methods, the fracture toughness may have seemed to be a material parameter, under the circumstances of the applied methods.

Due to the absence of the exact material parameters C_1-C_4 for the implementation of the material model, the results of this study can not be quantitatively compared to the experimental results. As the purpose of this study is to research the detailed mechanics and validity of the arising phenomena of the proposed model, this is of no significant influence on the results.

The mesh dependency, related to the damage/plasticity model of the bulk material, that was found in section 3.1.3, has also been noticed in [2] by the required amount of elements to achieve acceptable accuracy of the results. Highly concentrated shear stresses near the crack tip in the model cause for large plastic deformations in the bulk material, which requires extreme mesh refinement to achieve realistic results. For this reason, it is believed that a mesh independent result is achievable, although this will be impractical for larger or more complex models. The dependency influences the magnitude of the load at which crack propagation arises, but not so much the characteristics of it, which renders its impact on this research neglectable.

Modeling only a small part of the specimen for this study shows different load displacement diagrams compared to those of the experiment. A more distinct transition into crack growth is found in the results of the short model, which mostly disappears when modeling the full length of the specimen. These results coincide with those of the experiment, in which the elastic strain over the full length of the specimen partially hides the crack growth branch.

To answer the question whether the analytical approach of Eq. 2.1 is fit for the modified Transverse Crack Tension test with through the thickness compressive stress, to define the mode II fracture toughness, the answer is no.

The assumption for the analytical approach of Eq. 2.1 and 2.2 is a constant load until failure, in which the failure load is used to calculate the stress required for crack growth. This thesis has shown that there is a load range in which crack growth occurs, which makes the failure load dependent on the compressive stress and the length over which it is applied.

Because the TCT and mTCT test are based on energy dissipation effects to find the fracture toughness, all these effects influence the results. Adding friction to the model, influenced by a compressive stress, adds an energy dissipation effect. The constant fracture toughness per element, complemented by the cumulative traction on the interface of all damaged elements, changes the constant crack growth load into a load range.

From the results of this research can be concluded that the proposed model would be suitable for further investigation on the influence of compressive stresses in an mTCT test. Convergence was reached for all essential steps of the calculations and a good agreement was found with the experimental results, when modeling the full length of the right side of the specimen.

5.2 Recommendations

Some recommendations for further research can be made, based on this study. Results from these further research suggestions can give better insight into the validity of the proposed model as well as the phenomena that occur during failure under these circumstances.

For a quantitative comparison of the model results to the experimental results, an extreme mesh refinement study and an experimental campaign as in van Paepegem et al. [10] can be performed. The corresponding values for C_1-C_4 can then be fitted to the applied material and used in the material model. An alternative approach would be a plasticity model as proposed by Vogler et al. [11].

More experimental setups can be tested with the mTCT test, not only varying compressive stresses, but also varying pressure zone lengths. The influence of the pressure zone length in the model is significant for the results, which will have to be validated by these experiments. Since the crack propagation is found to occur under an increasing load, an alternative setup for the application of the compressive stress could provide the ability to register this crack growth through the model. A sufficiently stiff clamp on the outside of the steel grips of Figure 2.7, removing the need for bolts on each side of the sample, could be a possible setup.

Previous research [3] has already shown the difference in fracture toughness output from the mTCT test compared to the standardized tests. As the analytical approach for the fracture toughness as described by Eq. 2.1 and 2.2 is invalid for the case of through the thickness compressive stress, further studies on this part can be performed. An iterative process could be implemented, increasing the input fracture toughness of elements in front of the crack tip based on the compressive stress and fracture length in the compressed zone. This could remove friction from the material model and provide the possibility to start with a basic fracture toughness input value.

For an mTCT test on a specific sample, an adapted version of Eq. 2.1, including the compressive stress and pressure zone length on the specimen, could be fitted to coincide with the failure load. This would not represent the fracture toughness of the material, but merely the total energy dissipation required to form a crack in the last element in the compressed zone.

Bibliography

[1] M.R. Wisnom. On the increase in fracture energy with thickness in delamination of unidirectional glass fibre-epoxy with cut central plies. *Journal of Reinforced Plastics and Composites*, 11(8):897–909, aug 1992.

[2] F.P. van der Meer and L.J. Sluys. A numerical investigation into the size effect in the transverse crack tension test for mode II delamination. *Composite structures*, 54: 145–152, aug 2013.

[3] T. Scalici, G. Pitarresi, G. Catalanotti, F.P. van der Meer, and A. Valenza. The transverse crack tension test revisited: An experimental and numerical study. *Composite structures*, 158:144–159, dec 2016.

[4] T.A. Collings. The strength of bolted joints in multi-directional cfrp laminates. *Composites*, 8:43–55, jan 1977.

[5] G. Catalanotti, T. Scalici, G. Pitarresi, and F.P. van der Meer. The effect of the through-the-thickness compressive stress on the mode II interlaminar fracture toughness. *Composite structures*, 182:153–163, sep 2017.

[6] G. A. O. Davies, P. Robinson, J. Robson, and D. Eady. Shear driven delamination propagation in two dimensions. *Composites Part A: Applied Science and Manufacturing*, 28(8):757–765, jun 1997.

[7] A. Turon, P.P. Camanho, J. Costa, and C.G. Dávila. A damage model for the simulation of delamination in advanced composites under variable-mode loading. *Mechanics of materials*, 38(11):1072 – 1089, nov 2006.

[8] G. Alfano and E. Sacco. Combining interface damage and friction in a cohesive-zone model. *International Journal for Numerical Methods in Engineering*, 68(5):542 – 582, oct 2006.

[9] F.P. van der Meer, C. Oliver, and L.J. Sluys. Computational analysis of progressive failure in a notched laminate including shear nonlinearity and fiber failure. *Composites Science and Technology*, 70(4):692–700, jan 2010.

[10] W. van Paepegem, I. de Baere, and J. Degrieck. Modelling the nonlinear shear stress–strain response of glass fibre-reinforced composites. *Composites Science and Technology*, 66(10):1465–1478, jun 2006.

[11] M. Vogler, R. Rolfes, and P.P. Camanho. Modeling the inelastic deformation of polymer composites - part I: Plasticity model. *Mechanics of materials*, 59:50–64, apr 2013.